

Annual Report

Development of Stimulation Diagnostic Technology

*Prepared by:
Sandia National Laboratories*

Gas Research Institute

*Drilling and Completion Team
June 1997*

DEVELOPMENT OF STIMULATION DIAGNOSTIC TECHNOLOGY

ANNUAL REPORT
(January 1996-December 1996)

Prepared by
N. R. Warpinski,
J. E. Uhl,
B. P. Engler,
J. C. Lorenz,
C.J. Young,

Sandia National Laboratories
Division 6116
P.O. Box 5800
Albuquerque, New Mexico 87185

For
GAS RESEARCH INSTITUTE
Contract No. 5089-211-2059

GRI Project Manager
Steve Wolhart
Drilling and Completions Team

February 1997

REPORT DOCUMENTATION PAGE

Form Approved
OMB No. 0704-0188

Public reporting burden for this collection of information is estimated to average 1 hour per response, including the time for reviewing instructions, searching existing data sources, gathering and maintaining the data needed, and completing and reviewing the collection of information. Send comments regarding this burden estimate or any other aspect of this collection of information including suggestions for reducing this burden to Washington Headquarters Services, Directorate for Information Operations and Reports, 1215 Jefferson Davis Highway, Suite 1204, Arlington, VA 22202-4302, and to the Office of Management and Budget, Paperwork Reduction Project (0704-0188), Washington, D.C. 20503.

1. AGENCY USE ONLY (Leave blank)		2. REPORT DATE June 1997	3. REPORT TYPE AND DATES COVERED Annual Report, January 1996 to December 1996	
4. TITLE AND SUBTITLE DEVELOPMENT OF STIMULATION DIAGNOSTIC TECHNOLOGY			5. FUNDING NUMBERS GRI contract no. 5089-211-2059	
6. AUTHOR(S) N.R. Warpinski, J.E. Uhl, B.P. Engler, J.C. Lorenz, C.J. Young				
7. PERFORMING ORGANIZATION NAME(S) AND ADDRESS(ES) Sandia National Laboratories MS 0705 P.O. Box 5800 Albuquerque, New Mexico 87185			8. PERFORMING ORGANIZATION REPORT NUMBER SAND97-1327	
9. SPONSORING/MONITORING AGENCY NAME(S) AND ADDRESS(ES) Gas Research Institute 8600 West Bryn Mawr Ave. Chicago, IL 60631-3562			10. SPONSORING/MONITORING AGENCY REPORT NUMBER GRI-97/0115	
11. SUPPLEMENTARY NOTES				
12a. DISTRIBUTION/AVAILABILITY STATEMENT			12b. DISTRIBUTION CODE	
13. ABSTRACT (Maximum 200 words) The approach to stimulation diagnostics is to integrate in situ stress measurements (including microfracs, anelastic strain recovery, circumferential velocity analysis, and coring-induced fractures) with natural fracture characterization, stimulation analyses (including FRACPRO [®] , other models, finite-element analyses, and various pressure analyses), and fracture diagnostics in order to validate hydraulic fracture concepts, models and diagnostic capabilities. The M-site B-sandstone and C-sandstone experiments have provided the time evolution of a series of hydraulic fracture injections conducted in layered sedimentary sequences. Using a 30-level cemented-in receiver array and a 5-level wireline array in the two monitoring well, detailed measurements of fracture growth have been obtained for 12 fracture injections. These results show limited fracture height growth for initial water and linear gel injections, but considerable asymmetric height growth for a larger-volume, x-linked-gel, propped-fracture treatment. Comparison with models has shown some significant areas of disagreement. Both of these tests have provided validation of the accuracy of the microseismic technique for imaging fractures. Fracture height was validated using inclinometers, while azimuth and length were validated using intersection-well experiments. Studies of location schemes for microseisms have shown reasonable strategies (and the corresponding uncertainties) for using single-well, multiple-receiver arrays. Such schemes are being implemented in automatic processing codes for use in multi-level wireline systems. The wireline multi-level receiver system was successfully revamped to solve circuitry problems. Finite-element models for downhole tiltmeter behavior have been completed and used for M-Site studies. These models were used in the microseismic validation process to determine the effects of layer properties on the inclinometer results.				
14. SUBJECT TERMS Tight gas sands, in situ stress, stress measurement, natural fractures, hydraulic fracturing, hydraulic fracture diagnostics, microseisms, acoustic emissions, coring induced fractures, inclinometers, tiltmeters			15. NUMBER OF PAGES 63	
			16. PRICE CODE	
17. SECURITY CLASSIFICATION OF REPORT Unclassified	18. SECURITY CLASSIFICATION OF THIS PAGE Unclassified	19. SECURITY CLASSIFICATION OF ABSTRACT Unclassified	20. LIMITATION OF ABSTRACT	

GRI DISCLAIMER

LEGAL NOTICE This report was prepared by Sandia National Laboratories as an account of work sponsored by the Gas Research Institute (GRI). Neither GRI, members of GRI, nor any person acting on behalf of either:

- a. Makes any warranty or representation, express or implied, with respect to the accuracy, completeness, or usefulness of the information contained in this report, or that the use of any apparatus, method, or process disclosed in this report may not infringe privately owned rights; or
- b. Assumes any liability with respect to the use of, or for damages resulting from the use of, any information, apparatus, method, or process disclosed in this report.

Title	Development of Stimulation Diagnostic Technology
Contractor	Sandia National Laboratories GRI Contract Number: 5089-211-2059
Principal Investigator	N. R. Warpinski
Report Period	January 1996-December 1996 Annual Report
Objective	To apply Sandia's expertise and technology towards the development of stimulation diagnostic technology in the areas of in situ stress, natural fracturing, stimulation processes and fracture diagnostics.
Technical Perspective	Large quantities of natural gas exist in low permeability reservoirs throughout the US. Characteristics of these reservoirs, however, make production difficult and often uneconomic. Matrix rock permeabilities are often submicrodarcy, and natural fractures are commonly marginal, being anisotropic and easily damaged. Stimulation is required for these types of reservoirs, with hydraulic fracturing being the primary stimulation option. Understanding stimulation behavior is difficult, however, because of the complex nature of most of these reservoirs. Diagnostics that can map out the fracture length, height, and azimuth are the missing element in hydraulic-fracture analysis. Integrating knowledge of the matrix rock, natural fractures, in situ stresses with stimulation models and diagnostics is required if stimulation effectiveness is to be determined and enhanced.
Results	<p>Activities during 1996 centered on the M-Site experiment, where the principal activity was the documentation of the B sandstone experiments and the completion of all C-sandstone experiments. C sandstone experiments included fracture diagnostics on six fracture injections, including two linear-gel minifrac, 3 crosslinked-gel minifrac, and a propped treatment typical of these size of treatments typically pumped by local operators. The unique feature of these tests was the drilling of a deviated lateral well out ahead of the fracture and the subsequent monitoring of the pressure in the well to determine when it was intersected by the fracture.</p> <p>Sufficient high quality data were obtained from each injection that the growth history of the hydraulic fracture was developed for using microseismic techniques, but confirmed with downhole inclinometer data. There was excellent agreement between the length obtained from the microseismic data compared to the time of intersection of the lateral well.</p>

Microseismic results also showed a fracture-growth behavior that was dependent on the fluid and rates of the injection. Linear gels resulted in well-contained fractures, whereas tests using crosslinked gel always exhibited some height growth. Fracture lengths extended as much as 600 ft.

Hardware upgrades were made to the to the 5-level wireline receiver array. These instrumentation are now functioning reliably and accurately. Software programs to process data from these systems are being refined continually to accurately process data under varied conditions.

Finite element analyses of the B sandstone inclinometer results were completed and gave the final validation of the microseismic data. It was found that modulus variations in the thin layers has a significant effect on the inclinometer response and must be accounted for in highly layered environments.

Technical
Approach

The approach to stimulation diagnostics is to integrate in situ stress measurements (including microfracs, anelastic strain recovery, circumferential velocity analysis, and coring-induced fractures) with natural fracture characterization, stimulation analyses (including FRACPRO™ other models, finite-element analyses, and various pressure analyses), and fracture diagnostics in order to validate hydraulic fracture concepts, models and diagnostic capabilities. From now until the end of the project, the emphasis will be on developing a diagnostics system to map out hydraulic-fracture length and other parameters. The ultimate goal is to develop real-time, industry-run, fracture-diagnostics capabilities.

Project
Implications

The focus of this project is on stimulation diagnostics to be used for the optimization of hydraulic fracturing and field development. A key deliverable is to provide the foundation for a service to map hydraulic fractures using analysis of microseismic emissions from and near the hydraulic fracture. The use of microseisms to determine fracture geometry was validated at M-Site during tests conducted in the B-Sand and C-Sand. GRI and Sandia will begin field testing of the hydraulic fracture mapping service at other sites in 1997. The mapping service will be available for commercial use in 1998.

Steve Wolhart
Principal Project Manager, Drilling & Completion

TABLE OF CONTENTS

1.0	RESEARCH OBJECTIVES	1
2.0	SUMMARY OF ALL PREVIOUS WORK PERFORMED	3
3.0	SPECIFIC OBJECTIVES OF THE CURRENT YEAR	5
4.0	WORK PLANS FOR THE CURRENT YEAR	6
5.0	IN SITU STRESS	7
6.0	NATURAL FRACTURES	9
7.0	STIMULATION	10
8.0	M-SITE EXPERIMENT	11
9.0	MICROSEISMIC PROCESSING	48
10.0	OTHER DIAGNOSTIC TASKS	49
11.0	REFERENCES	50
12.0	MAJOR ACHIEVEMENTS	51
13.0	MAJOR PROBLEMS	52
14.0	CONCLUSIONS	53
15.0	OBJECTIVES AND WORK PLANNED FOR NEXT YEAR	54

Tables

1. Comparison of microseismic and intersection well azimuths	12
2. Summary of inclinometer finite-element calculations	18
3. Comparison of microseismic and inclinometer heights	19
4. Details of fracture injections	21

Figures

1. Example of tiltmeter response at initial re-opening of a hydraulic fracture	8
2. Location of intersection well 1B (1W-1B)	12
3. Example tiltmeter data as a function of time, minifrac 6B	13
4. Layer information for inclinometer finite-element code	14
5. Comparison of 5B & 6B inclinometer data with an analytic solution and finite element results	15
6. Comparison of finite-element and measured data for KCI injections	16
7. Comparison of 2D and 3D finite-element results	16
8. Geometry for 7B 3D finite-element analysis	17
9. Comparison of 3D propped fracture finite element results with actual data	18
10. Plan view of 1W-1C intersection well relative to other M-Site wells	20
11. Side view of C-sandstone intersection of 1W-1C	21
12. Pressure data for 1C injection	22
13. Plan view of all injection 1C microseisms	23
14. Side view of all injection 1C microseisms	23
15. Plan view of injection 1C microseisms recorded after 5 minutes (shut in)	24
16. Side view of injection 1C microseisms recorded after 5 minutes (shut in)	24
17. Plan view of injection 1C microseisms recorded after 10 minutes	25
18. Side view of injection 1C microseisms recorded after 10 minutes	25
19. Plan view of injection 1C microseisms recorded after 20 minutes	26
20. Side view of injection 1C microseisms recorded after 20 minutes	26
21. Plan view of injection 1C microseisms recorded after 30 minutes	27
22. Side view of injection 1C microseisms recorded after 30 minutes	27
23. Pressure data for 2C injection	28
24. Plan view of all injection 2C microseisms	29
25. Side view of all injection 2C microseisms	29
26. Plan view of injection 2C microseisms recorded after 5 minutes of testing	30
27. Side view of injection 2C microseisms recorded after 5 minutes of testing	30
28. Plan view of injection 2C microseisms recorded after 10 minutes of testing	31
29. Side view of injection 2C microseisms recorded after 10 minutes of testing	31
30. Plan view of injection 2C microseisms at the time of intersection of 1W-1C	32
31. Side view of injection 2C microseisms at the time of intersection of 1W-1C	32
32. P-wave tomogram of C sandstone region showing possible additional sandstone	33
33. S-wave tomogram of C sandstone region showing possible additional sandstone	34
34. Pressure data for 3C injection	35

35. Plan view of all injection 3C microseisms	36
36. Side view of all injection 3C microseisms	36
37. Plan view of injection 3C microseisms after 10 minutes of testing	37
38. Side view of injection 3C microseisms after 10 minutes of testing	37
39. Plan view of injection 3C microseisms after 20 minutes of testing	38
40. Side view of injection 3C microseisms after 20 minutes of testing	38
41. Plan view of injection 3C microseisms after 30 minutes of testing	39
42. Side view of injection 3C microseisms after 30 minutes of testing	39
43. Plan view of injection 3C microseisms after 40 minutes of testing	40
44. Side view of injection 3C microseisms after 40 minutes of testing	40
45. Injection 4C pressure data	41
46. Plan view of all injection 4C microseisms	42
47. Side view of all injection 4C microseisms	42
48. Plan view of injection 4C microseisms recorded after 90 minutes of testing	43
49. Side view of injection 4C microseisms recorded after 90 minutes of testing	43
50. Plan view of injection 4C microseisms recorded after 125 minutes of testing	44
51. Side view of injection 4C microseisms recorded after 125 minutes of testing	44
52. Plan view of injection 4C microseisms recorded after 140 minutes of testing	45
53. Side view of injection 4C microseisms recorded after 140 minutes of testing	45
54. Plan view of injection 4C microseisms recorded after 155 minutes of testing	46
55. Side view of injection 4C microseisms recorded after 155 minutes of testing	46

1.0 RESEARCH OBJECTIVES

The objective of this project is for Sandia National Laboratories to apply its expertise and technology towards the development of stimulation diagnostic technology. Stimulation diagnostic technology, as defined here, contains different areas such as (1) in situ stresses, (2) natural fracture characterization, (3) stimulation modeling, (4) hydraulic-fracture diagnostics, and (5) the design and conduct of field experiments. Integration of these areas can yield a more complete analysis of hydraulic fracture behavior and effectiveness in the reservoir. Beginning in the last quarter of this year, additional efforts were initiated to develop microseismic fracture diagnostics into a reliable, accurate, near-real time service.

In situ stresses, both the direction and the magnitudes, are of vital importance to the production of gas from low permeability reservoirs. Stress data are required for advanced design and analysis of fracture treatments, for completion information, and for understanding of the production mechanisms in tight reservoirs. The specific objective of the in situ stress task is to integrate core, log, and injection stress data into a complete picture of the stress in the reservoir, and to develop a "catalog" of techniques, each with a set of validated procedures, which can be brought to bear on the problem of stress determination.

Many of the tight reservoirs in the US, particularly in western basins, produce primarily from marginal natural fracture systems. Understanding the natural fracture system and the effects of stress, pore pressure, water saturation, etc., are important for any rational decisions on completion and stimulation of wells in these reservoirs. The specific objectives of the natural fracture task are to obtain description and distributions of the fracture systems from core, logs and outcrops, determine the importance of the fracture systems, and integrate these data for use in completion/stimulation design and production operations.

Effective hydraulic fracture stimulation requires a comprehensive design model that can adequately predict fracture behavior and reservoir performance. GRI has such a model (FRACPRO[®]) that can be used for design, analysis, and real-time control. Confident use of such models requires validation in realistic physical situations, a difficult task since the created fractures are not very accessible. The specific objectives of the stimulation modeling task are to perform analyses of injections using pressure analyses, finite element models, simple fracture models, and other resources in order to obtain a comparison with FRACPRO[®] and to aid in its validation.

Information on fracture behavior is currently available only through the use of indirect fracture diagnostic techniques, but these techniques are far from being routine field procedures, nor do they have the universal confidence of industry. The advancement of microseismic (and other seismic) monitoring requires rigorous standards for receivers, recorders, and processing algorithms. Completion of this task requires the application of advanced multi-station receivers that can faithfully record the particle motion induced by the specific events, the use of telemetry and recorders with sufficient dynamic range and band width to transmit and store the data, and the development of analysis techniques that can be applied in real-time or near-real-time modes.

Field experiments are an integral part of GRI's stimulation & completion research and the means by which models, diagnostics, and other procedures can be tested, refined, and verified. Sandia has a lead role in the diagnostic phases of the M-Site tests that are being conducted in the Piceance basin near Rifle, CO. This work includes the design of the instrumentation string of accelerometers and tiltmeters for a newly drilled monitor well and the application of wireline microseismic instrumentation for existing wells. These field experiments will provide the baseline information for developing the hardware and processing algorithms for fracture diagnostic analysis.

In addition to the M-Site activities, Sandia will be jointly conducting other field experiments with interested companies in other locations. These tests will allow for data to be obtained in other formations with different properties, stresses, depths, etc., and they will also serve as test sites for technology developed under this project.

2.0 SUMMARY OF ALL PREVIOUS WORK PERFORMED

2.1 In Situ Stress

Previous work on in situ stresses includes ASR analyses of SFE-4, Canyon Sands, and UPRC Frontier core, and Circumferential Velocity analyses of the same core plus Maxus Cleveland formation and Berea core. In addition, detailed core measurements of stress and material properties were made on M-Site sandstone sample. A core-based stress-measurement report (GRI-93/0270)¹ and a follow-up stress-azimuth report (GRI-93/0429)² were prepared as part of this work.

2.2 Natural Fractures

Previous natural fracture studies include Green River basin fieldwork which identified two primary fracture sets and efforts to reconstruct the tectonic development of the basin which led to the development of the fractures. These results have been documented in two topical reports (GRI-94/0020 and GRI-95/0151) covering the Green River basin. Studies of natural fractures in core were used to develop a theory of the role of diagenesis in fracture development. This theory has proved useful in explaining Frontier fracture systems.

2.3 Stimulation

Previous stimulation activities include most importantly the analysis and documentation of the Fracture Propagation Modeling Forum results. These data were included in an SPE paper (SPE 25890) and GRI report (GRI-93/0109) summarizing the results. Other modeling activities have been conducted to assess site suitability and for comparison with M-Site results.

2.4 Diagnostics

A considerable effort in fracture diagnostics was conducted in 1992 at the M-Site during the site suitability testing and in 1993 at the M-Site during the "A" sand experiments. These experiments form the basis for all of the M-Site design work and the development of processing codes for fracture diagnostics.

The suitability testing was performed in order to assess whether the M-Site near Rifle was acceptable for fracture diagnostic research. Results from that test were highly positive, indicating that microseisms were generated in large numbers, they were highly analyzable, and they could be used to map fracture progress.

The "A"-Sand Multi-Level and Treatment-Well Diagnostic Tests was conducted in October-November of 1993. These tests included a detailed velocity survey and four fracturing experiments monitored with a four-level receiver system in an offset well and a single receiver (or other instrumentation) in the treatment well. Results showed a very asymmetric fracture with considerable height growth.

Instrumentation for the new M-Site monitor well were designed and emplaced during 1994. These instrumentation included 30 triaxial receiver arrays and 6 biaxial inclinometer arrays that were grouted in the new monitor well at M-Site. Initial check-out of the instrumentation showed extremely high noise levels due to the rural power system and large amount of drilling activity in the area. These noise problems were solved by:

- designing and fabricating new amplifier and power-supply systems that were highly shielded from the both electric and magnetic fields
- providing electric and magnetic shielding for all surface cable runs
- using isolation transformers on all instrumentation
- using battery power for all power supplies

The B sandstone experiments were conducted in 1995, although analysis continued into 1996. Seven separate fracture injections were conducted and monitored using microseismic and inclinometer arrays. Except for the initial

breakdown injection, sufficient microseismic diagnostics were obtained to construct video images of fracture growth with time and pressure.

After the breakdown, the three following injections were water fractures which resulted in contained fracture behavior and rapid lateral growth out to lengths of almost 400 ft for volumes up to 200 bbl. The two subsequent injections were linear-gel minifrac which initiated similarly to the water fracs, but eventually experienced some height growth when net pressures became large enough. These minifrac had injected volumes of 400 bbl.

Finally a propped fracture treatment was conducted using about 600 bbl of crosslinked gel and 80,000 lb of sand. This test was considerably more complicated than the earlier injections. The fracture initiated much like the linear-gel minifrac, but pressures rose significantly above those observed during the minifrac and considerable height growth occurred.

To validate the fracture heights using inclinometers (downhole tiltmeters), analytic models were developed for 2-D, radial, and flat elliptic cracks. These models were implemented in a real-time inclinometer monitoring program which plots tilt as a function of time and as a function of depth. The analytic models can be superposed on the tilt data and parameters can be varied to obtain an acceptable match of the models with the measured data. At the end of 1996, implementation of a finite-element tilt code was initiated to examine the effects of modulus layering.

An algorithm by Vidale and Nelson was chosen as the best tool for advanced analysis of microseisms in complicated layered media. This algorithm solves the Eikonal equations to determine the travel time from each receiver to every point in a grid space encompassing the microseismic volume of interest. The results are stored in files for each receiver and for each phase (e.g., p and s waves). When arrival time data for an event have been determined, a minimization routine is used to determine the best fit location to match the arrival times. This routine is guaranteed to find an absolute minimum, unlike most other algorithms which may stop at a local minimum. This code can also be ported to a personal computer and used for field processing.

Several codes have been developed for analyzing inclinometer data from M-Site. These codes are all analytic and include a radial fracture, a 2-D fracture and a 3-D flat elliptic fracture. These solutions are implemented in real-time processing codes at M-Site.

3.0 SPECIFIC OBJECTIVES OF THE CURRENT YEAR

Specific objectives of the current year are:

Complete analysis of M-Site B sandstone experiments and prepare documentation of those results, including SPE papers and final reports.

Begin technology transfer seminars of the B sandstone results.

Design and conduct M-Site C sandstone experiments. These experiments are more complicated than the B sandstone tests as they will attempt to intersect a lateral deviated well drilled out ahead of the hydraulic fractures. The information obtained from the intersection will be used to validate microseismic fracture lengths and examine fracture pressure drops.

Begin the analysis of M-Site C sandstone experiments.

Redesign printed circuit in five-level system to solve electrical problems. These problems surfaced during B-sandstone work and are due to poor workmanship in the population of the high-temperature circuit boards.

Perform finite-element analyses of M-Site B-sandstone inclinometer results. These analyses will provide the final comparison between inclinometer and microseismic heights and will account for both stress and modulus layers.

Develop/refine software codes for the automatic processing of microseismic data. Most importantly, work will begin on automatic processing of the s wave.

4.0 WORK PLANS FOR THE CURRENT YEAR

Work plans for the current year include:

Complete all QA work on M-Site B-sandstone microseismic locations. Prepare maps and visualizations of all of these tests and complete documentation in a final report and SPE paper. Begin performing technical seminars on the B-sandstone results and the implications for fracturing.

Design and fabricate printed circuit boards for the five-level system -- including the motor control board, the signal processing board and the A/D board – using 125°-C rated components and boards. The implementation of the new circuitry will be prior to their use in the C sand experiments.

Design M-Site C-sandstone experiments to monitor the intersection of a deviated lateral well by hydraulic fractures. Primary design questions are the location and deviation of the lateral well.

Conduct M-Site C-sandstone fracture experiments including cross-linked gel breakdown, linear-gel minifrac, crosslinked-gel minifrac and an industrial size stimulation treatment. Primary instrumentation includes:

- microseismic monitoring using the 30-level monitor-well accelerometer array and the five-level wireline accelerometer array;
- inclinometer monitoring using the 6-level monitor-well inclinometer array; and
- pressure monitoring in the intersection well.

Begin analysis of the M-Site C-sandstone experiments for microseismic locations, length validation, growth mechanisms and other important aspects of the tests.

Continue the refinement of SMART5, the automatic processing system for microseismic detection and location.

Continue the development of advanced codes for microseismic location algorithms using both homogeneous and layered-earth models.

Conduct finite-element analyses of the M-Site B-sandstone inclinometer results to obtain the best possible height estimate for comparison with the microseismic data. These results show the accuracy of the microseismic method by comparing the microseismic-calculated heights with the mechanical heights, as deduced from inclinometer-measured deformation.

5.0 IN SITU STRESS

Knowledge of the directions and magnitudes of in situ stress are of vital importance to the production of gas from low permeability reservoirs. Stress data are used in the design and analysis of hydraulic fracture stimulations and are necessary for the understanding of parameters affecting production. However, in situ stresses are difficult to measure, and there is no commonly accepted practice for determining the stresses. As a result, there is often a lack of confidence in stress data from any one technique. In light of this reality, it is common sense to develop as many ways as possible to determine stress parameters.

Sandia has previously worked on integrating information from anelastic strain recovery (ASR), differential strain curve analysis (DSCA), circumferential velocity anisotropy (CVA), coring-induced fractures, log-derived wellbore effects, overcoring of archived core, and microfrac stress measurements in order to obtain an integrated program to provide the best possible stress measurement. These activities led to the preparation of two reports, Core Based Stress Measurements: A Guide to Their Application¹ (GRI-93/0270) and Techniques for Determining Subsurface Stress Direction and Assessing Hydraulic Fracture Azimuth² (GRI-93/0429). As a result of these capabilities, Sandia conducted several core-based measurements on samples from the M-Site monitor well.

5.1 M-Site Stresses Derived from Inclinometer Opening

The primary activity over the year relative to in situ stresses, however, was to examine the inclinometer data at M-Site for the purpose of evaluating in situ stresses. It was originally expected that the inclinometers would show a discrete point where the hydraulic fracture was clearly closed. However, the fracture closure process was found to be a smooth, continuous one which often leaves residual inclinations of 20-30% of the maximum recorded value at any station. This residual tilt is probably due to residual width in the crack, poro-elastic expansion due to increased pore pressure, and slight shifting of the formation in response to the hydraulic fracture (microseisms, which are shear slippages, provide proof that some re-adjustment of the formation is occurring). The smooth decrease in inclination suggests that the entire process is a very continuous one where no point can be construed to be the closure of the crack. Thus, the difficulty in choosing closure from a hydraulic-fracture stress test is to be expected since there is no closure point in the actual rock deformation.

Fortunately, the inclinometers can be used to determine closure stress upon reopening of a fracture. Figure 1 shows the beginning of an injection in the B sandstone using water pumped at a low rate (1 bpm) to measure the point at which the crack begins to dilate. In this case, the crack response, which begins at about 18.5 minutes, can be compared to the downhole pressure to obtain the closure stress, which for this sandstone is approximately 3050 psi. This technique was found to be successful in the C sandstone as well.

The procedure for obtaining the closure stress requires that the formation be already fractured or broken down in order that a closed conductive crack be present. Otherwise, a large breakdown pressure may be required to start fracturing and no closure-stress measurement can be obtained. Secondly, the injection rate must be relatively slow so that fluid can penetrate into the fracture and begin to reduce stress on the fracture wall in a continuous manner. Otherwise, a reopening pressure is likely to be obtained, which again will make it impossible to determine the closure stress. When done correctly, the opening of the fracture is easily identifiable and the closure stress readily obtained. It is also worth noting that the closure stress measured in this manner is relatively close to that measured using small volume hydraulic fractures and finding a closure stress using square-root-of-time plots, graphical techniques, or other conventional means.

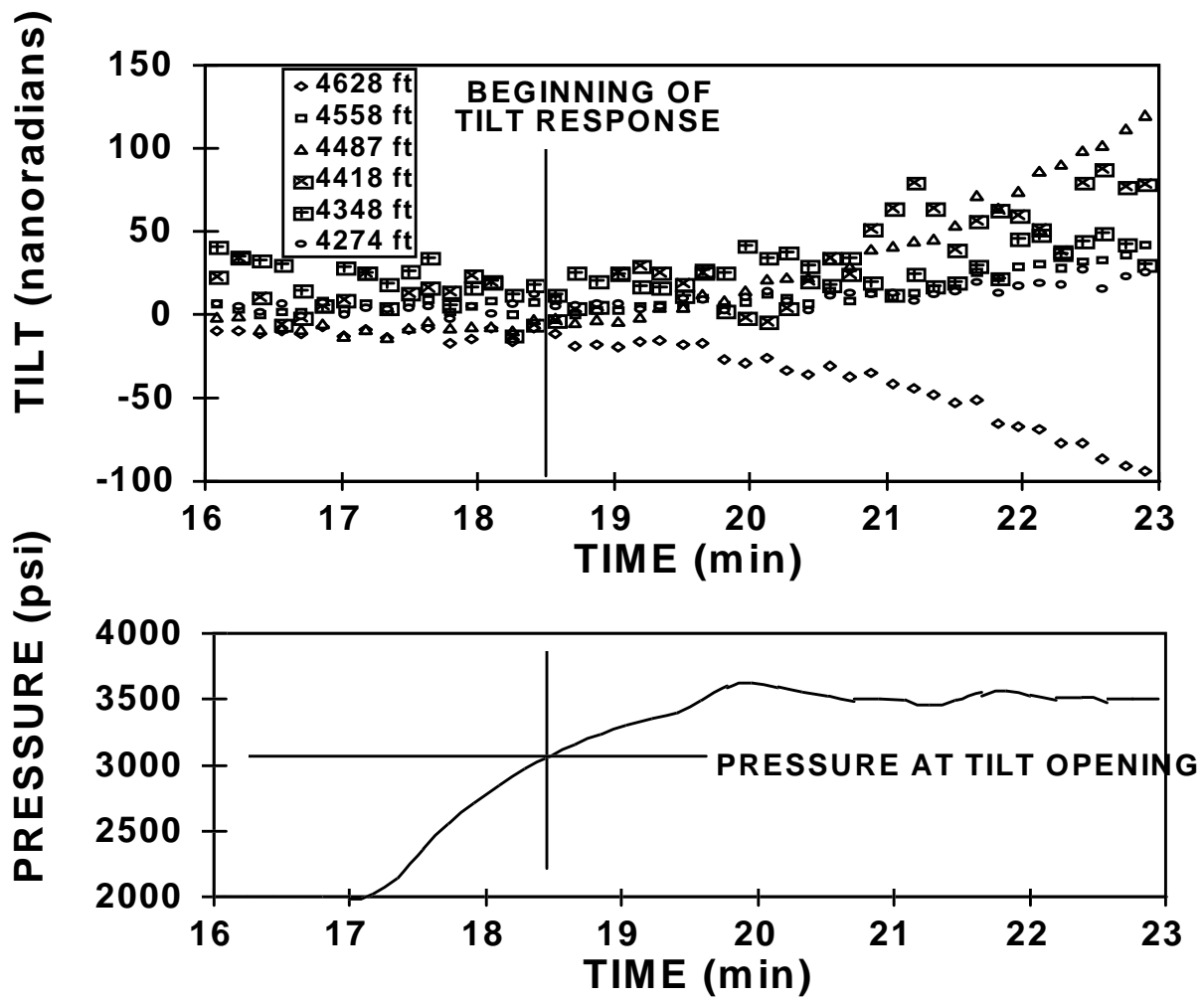


Figure 1. Example of tiltmeter response at initial re-opening of a hydraulic fracture

If even a single tiltmeter can be run in a borehole on a wireline, this technique can be used to determine an accurate closure stress, with the accuracy depending only on the distance between the fracture and the tiltmeter location. The tiltmeter, however, can be optimally placed at the point of maximum tilt, which can be estimated a priori.

6.0 NATURAL FRACTURES

Many of the tight sandstones, particularly those in western US basins, have matrix permeabilities of a few microdarcies or less. Economic production from such reservoirs is impossible unless natural fractures or other mechanisms provide additional permeability. Well testing of many of these microdarcy or submicrodarcy reservoirs often yields effective permeabilities of tens or hundreds of microdarcies, substantiating the hypothesis that most of these reservoirs are fractured. Outcrop, log and core studies have also shown the presence of natural fractures. Knowledge of the characteristics and importance of the natural fractures is important because it may affect the stimulation or other completion plan. Only limited activities were conducted on this task in 1996.

6.1 General Activities

Sandia participated in a partially GRI-funded test with Amoco Production Company to examine natural fractures found in a deep Frontier formation well. Production of gas from the 18,300-ft deep Frewen #4 Deep well in the eastern Green River basin (Wyoming) was uneconomic despite the presence of numerous open natural fractures in core taken from the well. Examination of the fractures in core suggested several reasons for the poor production and eventual abandonment of the well:

- Plugging of fracture permeability by residual pyrobitumen found in the natural fractures and matrix, and
- Reorientation of the in situ compressive stress such that fracture apertures become narrower or even shut during pressure decline.

The effective reservoir conductivity, despite numerous natural fractures, is limited by the matrix permeability which is only a few thousandths of a millidarcy.

7.0 STIMULATION

Some form of stimulation, usually hydraulic fracturing, is required for the economic production of gas from tight reservoirs. A long-sought objective has been comprehensive hydraulic-fracture models that could be used for the design, analysis, and, ultimately, real-time control of the fracturing process. In order to help validate such comprehensive models, Sandia is tasked to (1) analyze appropriate field stimulation and minifrac data in order to obtain an independent assessment of fracture performance, and (2) conduct any advanced activities (e.g., finite element analyses, model comparisons, etc.) which provide independent confirmation of model validity.

The only activity associated with stimulation during 1996 was the providing of M-Site data to several groups who requested the use of these data for their own model comparisons.

8.0 M-SITE EXPERIMENT

Three of the primary goals of GRI's Stimulation and Completion program are (1) validation of hydraulic-fracture design models, (2) development of hydraulic-fracture length diagnostics, and (3) validation of all fracture-diagnostic technology. Validation implies a confirmation of the predicted results by actual measurement in the field, and thus requires an instrumented facility where fracture behavior can be measured. The effort to develop such a capability is named the M-Site Experiments. Sandia has been involved (along with CER Corp., Branagan & Assoc. and RES) in the development and testing at M-Site.

The M-Site location is in the Piceance basin near the town of Rifle, CO, in Mesaverde sandstones at depths from 4000-5000 ft. Two wells, designated MWX-2 and MWX-3, are currently available for testing and fracturing and are shown in Figure 2. During the fall of 1992, a site suitability test was conducted, from which highly positive results were obtained. During 1993, the first of several experiments was conducted in the A sand, and planning for a new monitor well was initiated. During 1994, the monitor well was drilled and instrumentation installed. Work in the B sandstone began in 1995, during which time seven injections were conducted. Work in the C sandstone was completed during 1996.

8.1 B-Sandstone Experiments

The B-sandstone experiments consisted of a series of calibration injections conducted in April, 1995, a crosswell survey initiated in late July, 1995, two minifrac conducted in early August 1995, a propped fracture treatment conducted in late August 1995, and the drilling of an intersection well in the fall of 1995. Most analyses of B-sandstone fractures occurred during 1995, but some activities associated with comparisons with the intersection well were completed in 1996, as well as most of the finite-element studies of the inclinometer data. Reports and SPE papers documenting these results were also prepared during 1996. The SPE papers include:

- Branagan, P.T., Peterson, R., Warpinski, N.R. and Wright, T.B., "The Characterization of Remotely Intersected Set of Hydraulic Fractures: Results of Intersection Well No. 1: GRI/DOE Multi-Site Project," SPE 36452, SPE Annual Tech. Conf. & Exhibition, Denver, CO, Oct. 6-9, 1996.
- Branagan, P.T., Warpinski, N.R., Engler, B.P., Wilmer, R., "Measuring the Hydraulic Fracture-Induced Deformation of Reservoir and Adjacent Rocks Employing a Deeply Buried Inclinometer Array: GRI/DOE Multi-Site Project," SPE 36451, SPE Annual Tech. Conf. & Exhibition, Denver, CO, Oct. 6-9, 1996.
- Peterson, R.E., Wolhart, S.L., Frohne, K.-H., Warpinski, N.R., Branagan, P.T. and Wright, T.B., "Fracture Diagnostics Research at the GRI/DOE Multi-Site Project: Overview of the Concept and Results," SPE 36449, proceedings, 1996 SPE Annual Tech. Conf. and Exhibition, Denver, CO, October 6-9, 1996.
- Warpinski, N.R., Wright, T.B., Uhl, J.E., Engler, B.P., Drozda, P.M. and Peterson, R.E., "Microseismic Monitoring of the B-Sand Hydraulic Fracture Experiment at the DOE/GRI Multi-Site Project," SPE 36450, proceedings, 1996 SPE Annual Tech. Conf. and Exhibition, Denver, CO, October 6-9, 1996.

8.1.1 B-Sandstone Microseismic/Intersection Comparison

One of the primary unknowns associated with the microseismic technique is the accuracy of the geometry due to the relationship between the microseismic events compared to the fracture itself. As discussed previously, mechanical models suggest that the microseisms form a tight ellipsoid surrounding the fracture, but such an analysis has never been verified. Furthermore, unknown velocity structure inhomogeneity may also result in errors in locating the microseisms and predicting fracture geometry.

The B-sandstone intersection well, which located the hydraulic fracture using FMS and gamma logs, provides concrete information on the actual azimuth of the fracture compared to the microseismic azimuth. Table 1 below gives the microseismically monitored fracture azimuths for the six tests with adequate data. The average azimuth is N75°W while the median value is N74°W. The actual intersection azimuth is N72°W. Considering that this formation is a highly layered environment with significant velocity structure, these results show an excellent comparison.

Table 1. Comparison of microseismic and intersection well azimuths

Fracture Experiment	Microseismic Azimuth (deg)	Intersection Azimuth (deg)
2B	N76W	N72°W
3B	N74W	
4B	N77W	
5B	N74W	
6B	N74W	
7B	N74W	

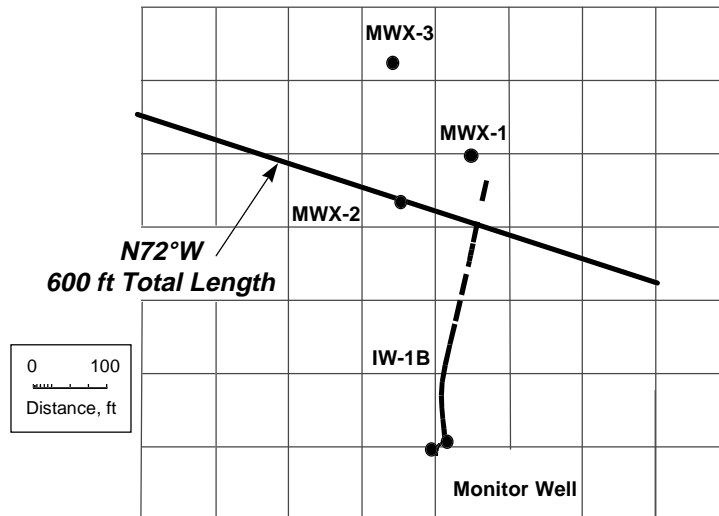


Figure 2. Location of intersection well 1B (IW-1B)

8.1.2. Inclinator Modeling of B-Sandstone Hydraulic Fractures

The bi-axial inclinometers cemented in place in the monitor well were installed principally to validate the fracture heights determined using microseisms. This validation was necessary because of uncertainty regarding the correlation between the seismic heights and the mechanical heights of the fractures. The inclinometers, or downhole tiltmeters, measure the gradient of strain, but the deformation behavior can be formulated in terms of the strain gradients as easily as the strains, so essentially the same information is available. The reason for using tiltmeters is that they are designed for extremely sensitive measurements, they are a well-known technology, they are already available for underground emplacement (although this application is much deeper than normal use), and there are no stress or strain meters that appeared suitable for these conditions. An example of the tiltmeter data obtained from the B6 minifrac is shown in Figure 3.

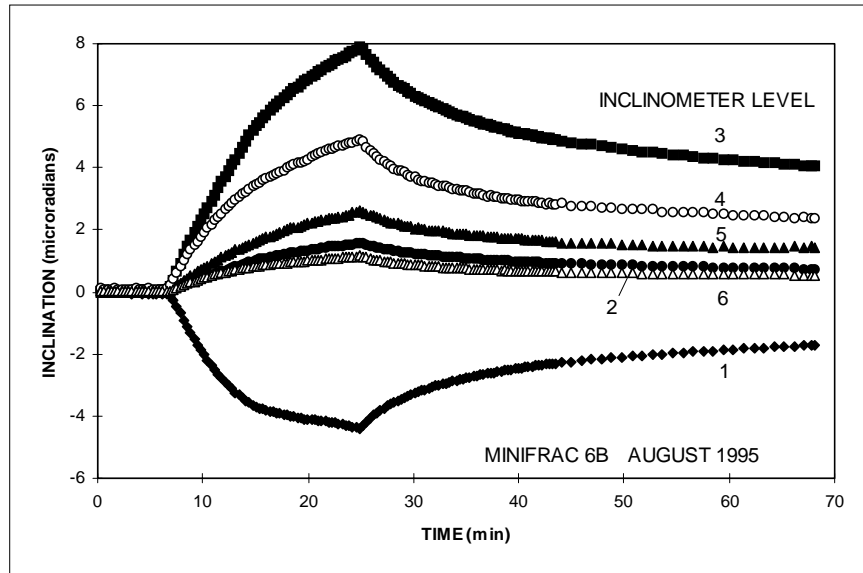


Figure 3. Example tiltmeter data as a function of time, minifrac 6B.

B-sandstone inclinometer data were gathered on all fracture injections and immediately compared with the analytic models to deduce height and other parameters. However, it was found that the analytic models did not adequately reproduce the measured tilt data. It was believed that the discrepancy was caused primarily by modulus variations within the layers, a feature that could not be accounted for by the analytic models. As a result, a series of finite-element analyses were performed using the JAC code.⁸

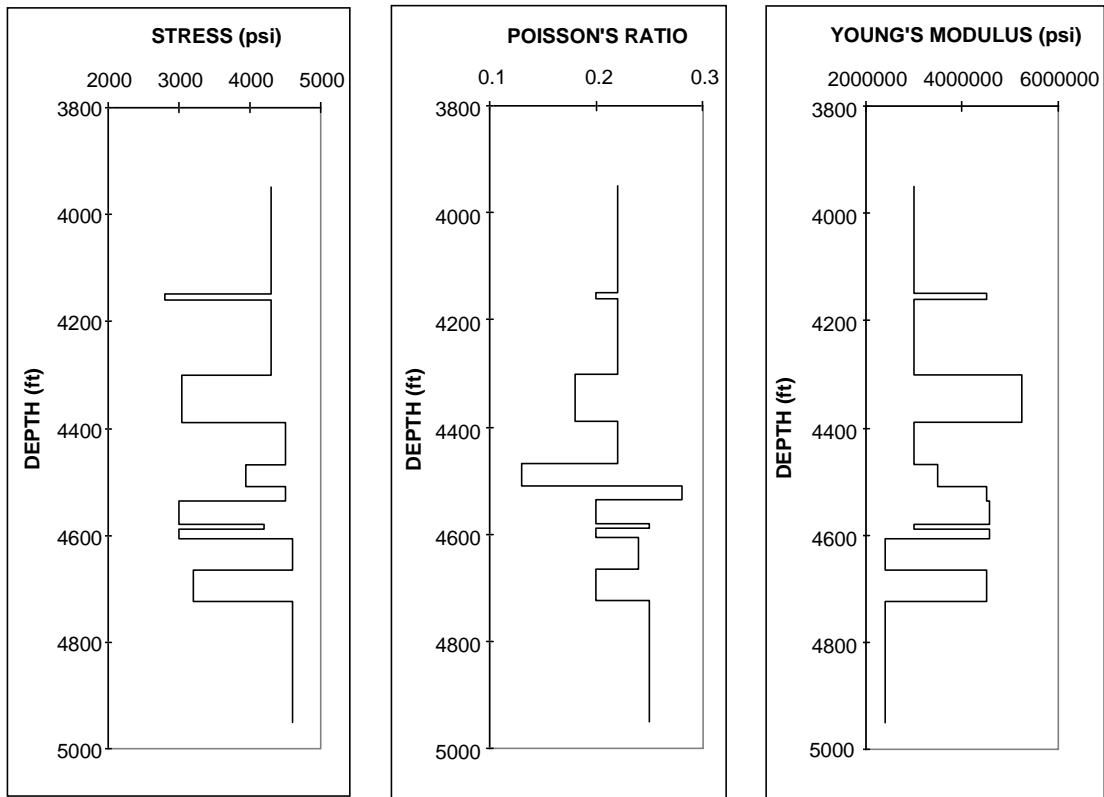


Figure 4. Layer information for inclinometer finite-element code

The analysis code was run on a 1000 ft x 1000 ft x 1400 ft geometry with the fracture length being in the 1400 ft direction. The depth covered was 3951 to 4951 ft, with 13 separate layers having different stress and moduli. There were 42,280 elements and 47,880 nodes in the model, with typical runs taking about 2 hr on a workstation. External boundary conditions were zero displacement, with the exception of the hydraulic fracture which had a constant pressure or pressure distribution (e.g., fracture 7B had a pressure distribution) on the fracture face.

These computer simulations were started with 2D runs (1000 ft x 1400 ft) to determine approximate sizes as well as refine the number of layers used in the simulations. Most of the initial runs used the minifrac as the test case, as they had relatively long length (fit the 2D assumption) and nearly constant height along their length, as determined from microseismic data. Eventually, 13 layers were used in the model, which encompass all of the major lithological units and whatever moduli data were available from MWX work and subsequent coring of the monitor well itself. Figure 5 shows a comparison of the actual inclinometer data for fractures 5B and 6B with the analytic 2D model and the best finite-element 2D model.

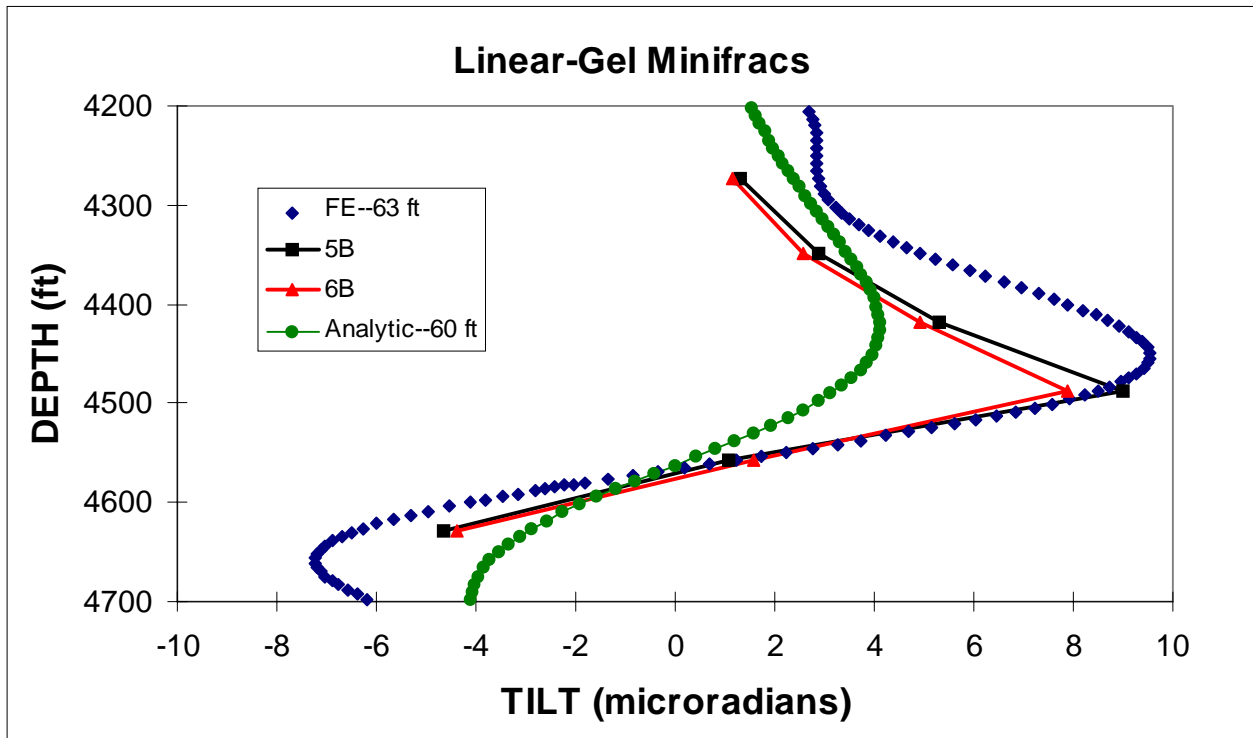


Figure 5. Comparison of 5B & 6B inclinometer data with an analytic solution and finite element results

As can be seen in Figure 5, the analytic solution can not represent the actual data very well. If the match is made on the peak values of the measured inclinations, then the match on the long-distance fall-off (top part of graph) is poor. If the match is made on the long-distance fall-off, then the matches of the peak values are poor. As seen in Figure 5, the discrepancy can be accommodated by the use of finite element models and the introduction of the appropriate layering.

The same layering developed for the minifrac matches was also used for the two primary KCl injections, 3B and 4B. The best fit match of the data occurred for a fracture height of 52 ft, essentially contained within the B sandstone. Figure 6 shows the comparison of the finite-element and measured tilt data.

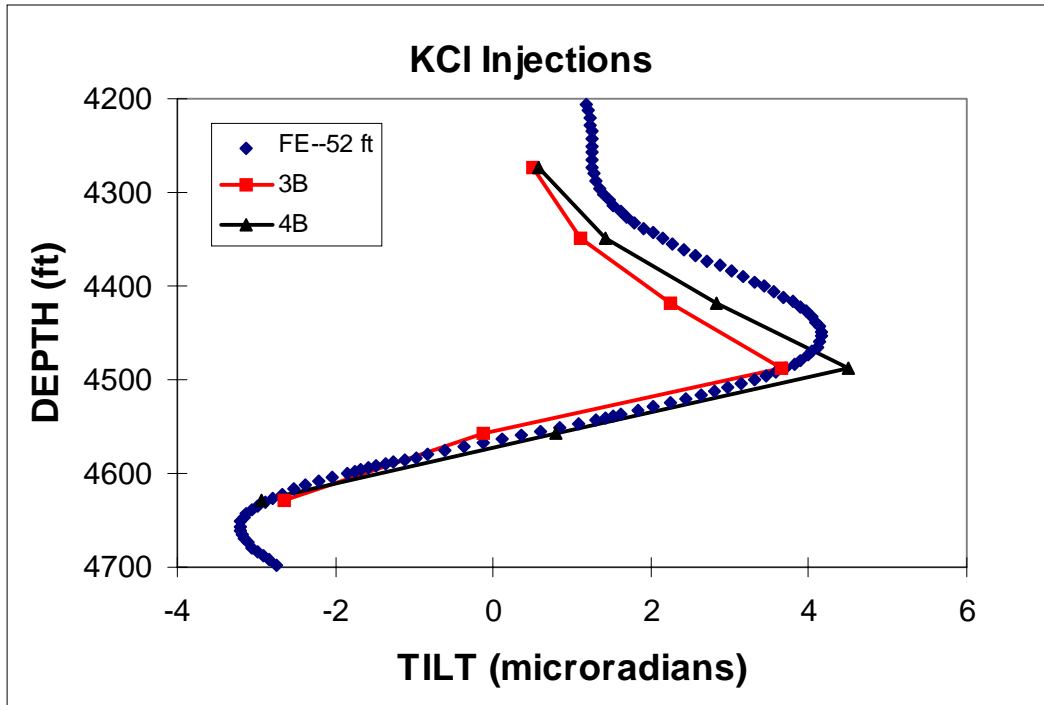


Figure 6. Comparison of finite-element and measured data for KCI injections

After obtaining reasonable 2-D matches on the KCI injections and the minifrac (the propped frac could not be run in 2D because of its non-constant height profile), 3-D calculations were performed and the height was adjusted to re-achieve the match. The final minifrac match had a net pressure of 1300 psi, a height of 67 ft, and a length of 350 ft. As shown in Figure 7, the shape of the curve is only slightly affected for a full 3D geometry and the height of the fracture had to be increased by only 6% to account for the non-infinite length of the fracture.

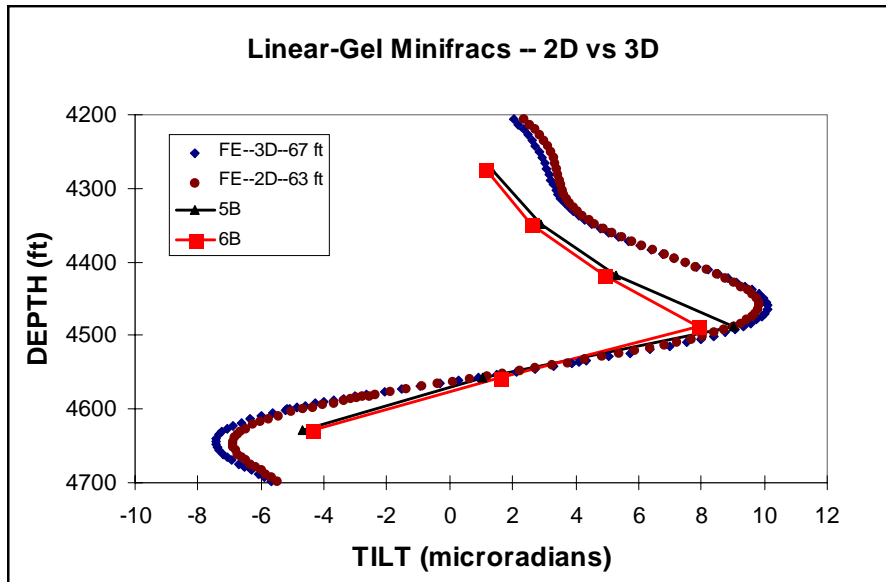


Figure 7. Comparison of 2D and 3D finite-element results

The propped fracture was a separate problem, because of both the non-constant height and the question of the true net pressure to use. 2-D calculations of the propped fracture with 2000 psi gave fracture heights on the order of 65 ft

to match the measured tilts. 2-D calculations with net pressures of 1400-1500 psi gave fracture heights of about 70-80 ft to match the measured tilts. Thus, there was no direct manner to match the microseismic data with its variable shape. For this problem, the methodology was turned around and the microseismic shape was assumed to be correct. Then, the height near the wellbore, the net pressure, and other parameters were adjusted until a reasonable match was achieved. Figure 8 shows the geometry as input into the finite-element model, as compared with the microseismic data taken for this injection. Only the right side (east wing) is shown because the inclinometer array is located on this wing.

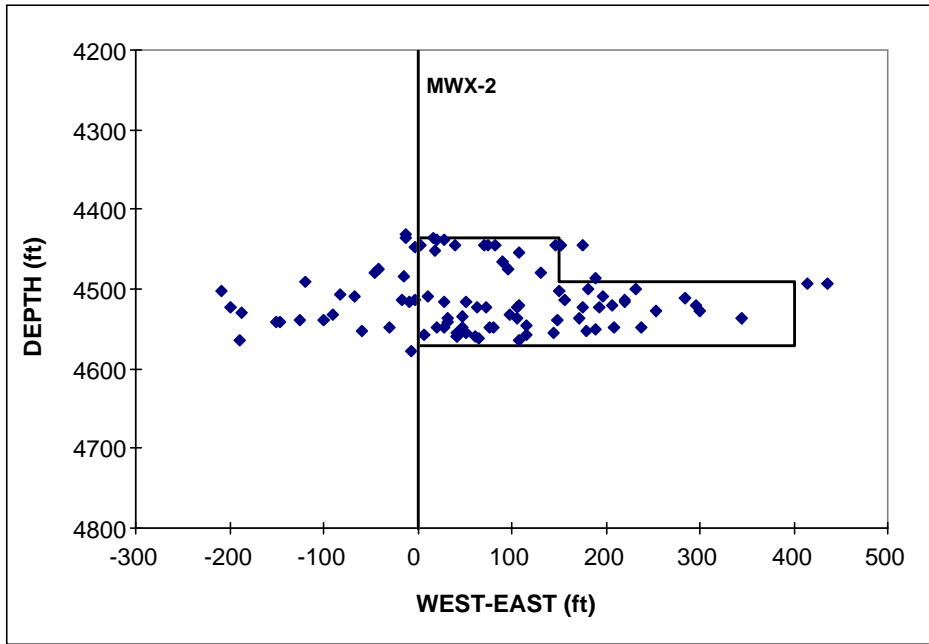


Figure 8. Geometry for 7B 3D finite-element analysis

One additional feature was added for this simulation. There is information that suggests that the net pressure in the bulk of the fracture is on the order of 1400-1500 psi, and such a reduced net pressure was actually used in the analysis. However, there was a question if there would be any effect from a near-wellbore zone where the pressure drops from 2000 psi to 1400 psi. To achieve this, a pressure drop region near the wellbore was added to the code and the resultant tilts were calculated. The final match, given all of these features, is shown in Figure 9. The match is clearly very good and suggests that the microseismic results accurately depict the fracture.

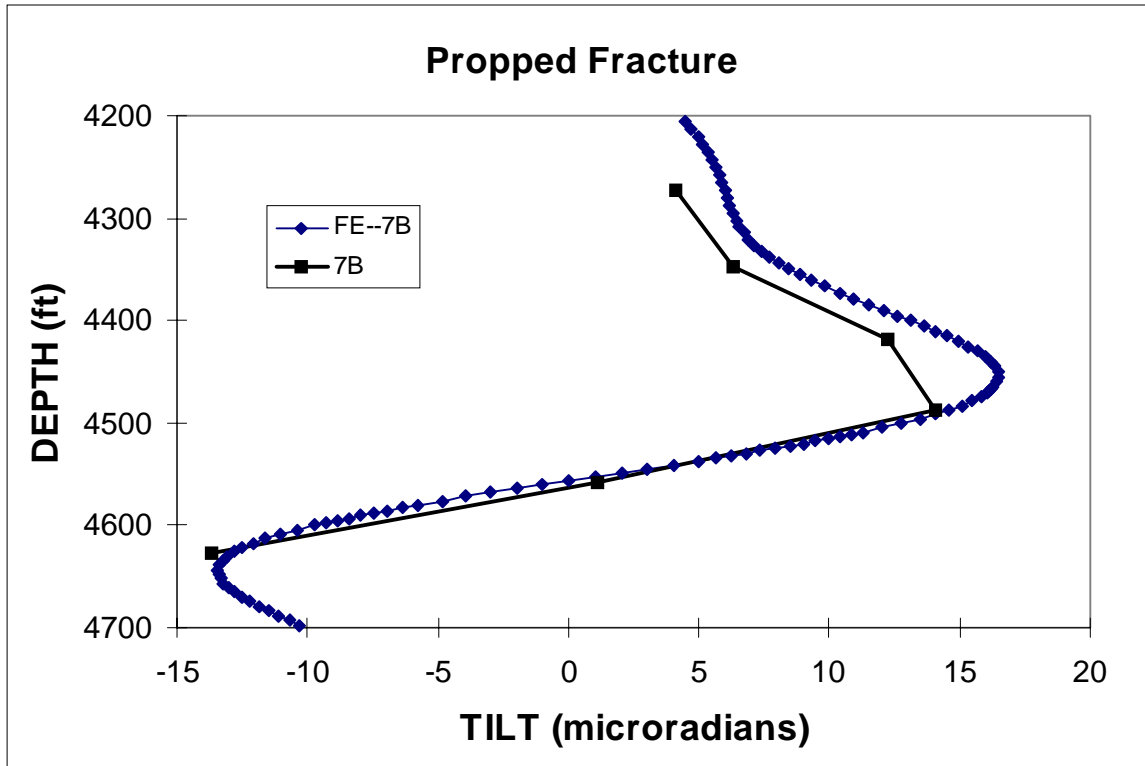


Figure 9. Comparison of 3D propped fracture finite element results with actual data

A summary of the results is shown in Table 2. The 2-D results have an infinite fracture length and no 3D case was run for the KCl injections because the change in height appeared to be only about 2-3 ft. The two heights and lengths for the 3-D propped fracture are for the near wellbore region, which is 135 ft high but only extends 150 ft, and for the far fracture region, which has an 80 ft height and extends to 400 ft.

Table 2. Summary of inclinometer finite-element calculations

Frac	Net Pressure	2-D Height	3-D Height	3-D Length
KCl fracs	1000	55	--	
Minifrac	1300	63	67	350
Propped Frac	1400	70-80	135 & 80	150 & 400

Important points that were found while performing these analyses:

- The tiltmeter results are very sensitive to height and modulus. If the modulus is decreased by any significant amount, the height must also be decreased as well or the calculated tilts are much too large. This fact suggests that the static core moduli used for these calculations cannot be lower or the fracture heights would be ridiculously small.
- Although much larger heights could be obtained if the moduli were considerably greater (as dynamic moduli typically are), larger moduli are difficult to accommodate as the greater heights force the peaks in the inclination data to move farther from the center fracture, thus not matching the data.
- The log dynamic moduli do not compare with dynamic moduli measured from the crosswell survey. The crosswell moduli are taken at much lower frequencies than logs or typical ultrasonic lab tests, and they agree very well with the static core measurements. If dynamic moduli from the crosswell survey are used in the finite analyses, the agreement is relatively good. The problem with the crosswell dynamic data is that there is not sufficient fine-scale resolution of the layers (10 ft grid spacing on the tomogram).

- 3D effects are typically about 10% different when the fracture length exceeds 350 ft (minifrac and main fracture). The calculations show that layering effects are about another 15%, so the total uncertainty in using a homogeneous model is no more than 25%, or about 20 ft for the minifrac and 40 ft for the main fracture (however, for the main fracture a 2D calculation would miss the shape variations of the fracture).
- A pressure distribution in the fracture was used in a few calculations, but there was only a very small difference. This feature was dropped for all final calculations.
- The tilts were found to be insensitive to Poisson's ratio.
- Fracture dimensions for the propped fracture are non-unique because of the non-constant height and uncertain net pressure. However, a match has been obtained using the seismic geometry and one assumption about the pressure in the propped fracture.
- In general, there is excellent agreement between tiltmeters and microseismic results.

8.2 B-Sandstone Microseismic Results

Although most of the B sandstone analyses were conducted in 1995, final quality assurance and limited playback of the data were performed during 1996. There were no significant changes to any of the data associated with these additional analyses and the microseismic images given in the 1995 annual report are essentially correct. However, after completing the inclinometer finite-element calculations, a comparison of the microseismic and inclinometer derived heights has been compiled and is shown in Table 3. These results show that the "seismic" height compares well with the mechanical height, as determined from the deformation of the rock mass.

Table 3. Comparison of microseismic and inclinometer heights

TEST	SEISMIC	INCLINOMETER
B3	55	52
B4	55	52
B5	80	67
B6	75	67
B7	135	135

8.3 C Sandstone Experiments

C sandstone experiments were conducted during the July 1996 to December 1996 time frame, after which the site was permanently shut down. The C sandstone experiments were considerably different from the B sandstone tests in that the intersection well was drilled prior to fracturing to provide data on both time of intersection and type of intersection. The objectives of the C sandstone experiments were

- Validate fracture length from microseisms using the intersection well to provide time of arrival information (by monitoring the pressure) which could be directly correlated with the microseisms at that time.
- Validate microseismic azimuth by providing a direct measurement of the intersection location.
- Provide modeling validation on fracture length in the same manner as the microseismic comparison.
- Provide information on mechanisms by measuring intersection well pressures and imaging the fractures created in the intersection well.
- Provide inclinometer information on fracture deformation to validate both models and microseisms and to give other useful information on closure, prop distribution, residual deformation and other features.

8.3.1 Layout of C sandstone wells

The C sandstone lateral well was drilled during July of 1996. A plan view of the intersection is shown in Figure 10, while the details of the intersection are shown in side view in Figure 11. The intersection well cuts through the expected fracture plane about 300 ft from the treatment well.

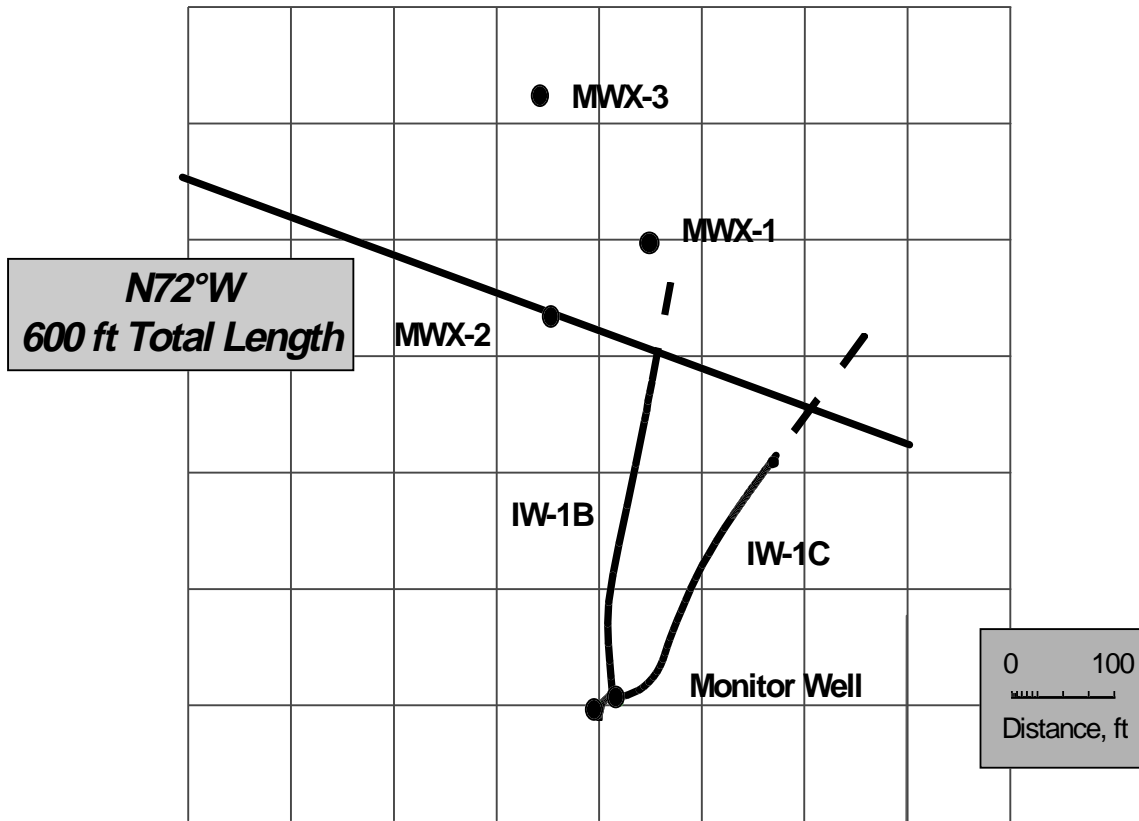


Figure 10. Plan view of IW-1C intersection well relative to other M-Site wells.

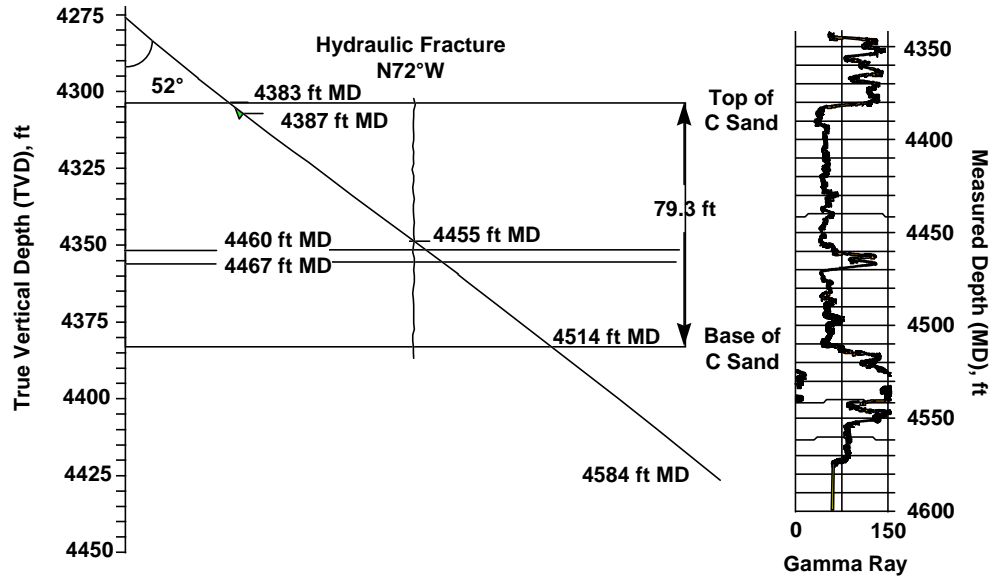


Figure 11. Side view of C-sandstone intersection of IW-1C.

8.3.3 C sandstone fracture experiments

The C sandstone fracture experiments consisted of six injections conducted between August 1996 and December 1996, including a crosslinked gel breakdown, two linear gel minifracs, two crosslinked gel minifracs and a final propped treatment. Table 4 shows important details of these injections. The fifth column notes where the 5-level wireline seismic array was located, although it failed in the treatment well in fracture 4C. The sixth and seventh columns note whether a gamma ray or FMS log was run in the intersection well after the injection, and the last column notes the lack of pressure communication (NONE), a slow rise in pressure (RISE), or a clear connection in to the wellbore with an associated rapid pressure increase (CONNECT). The microseismic results associated with these injections are discussed in the following sections.

Table 4. Details of fracture injections

TEST	FLUID GEL TYPE	RATE (bpm)	VOLUME (bbl)	5-LEVEL	IW-1C TRACER	IW-1C FMS	IW-1C PRESSURE
1C	X-LINK	20	100	MWX-3	NO	NO	NONE
2C	LINEAR	22	136	MWX-3	YES	YES	RISE
3C	LINEAR	24	250	MWX-3	YES	NO	RISE
4C	X-LINK	40	950	MWX-2	YES	YES	CONNECT
5C	X-LINK	30	645	MWX-2	NO	NO	RISE
6C	X-LINK	30	1750	MWX-3	YES	YES	RISE

Microseismic traces and hodograms are not shown in this report, as they are very similar to those obtained during B-sandstone injections. Many examples of the B-sandstone microseisms are given in the 1995 annual report (Development of Stimulation Diagnostic Technology, Warpinski et al.).

8.3.4 Injection 1C microseismic results

Injection 1C, which was conducted on August 6, 1996, was a 100 bbl breakdown using a crosslinked gel pumped at 20 bpm. The pressure behavior for this injection is shown in Figure 12, showing that the pressure steadily ramped up to about 4050 psi, which is a net pressure of 1000 psi (closure stress = 3050 psi). The total duration of the injection was 5 min, but microseisms were detected for 53 min. Figure 13 shows a plan view of the final geometry of the fracture, as measured from the microseisms. This figure indicates that the fracture azimuth is N75°W with wing lengths of approximately 200 ft. Data were obtained from both the cemented in monitor well to the south and from the 5-level wireline array in MWX3 to the north. It can also be seen that while there are more monitor-well data points, both arrays mark out relatively similar fracture lengths and orientations. One reason that more microseisms were observed in the monitor well than from the wireline array in MWX-3 is that MWX-3 had some

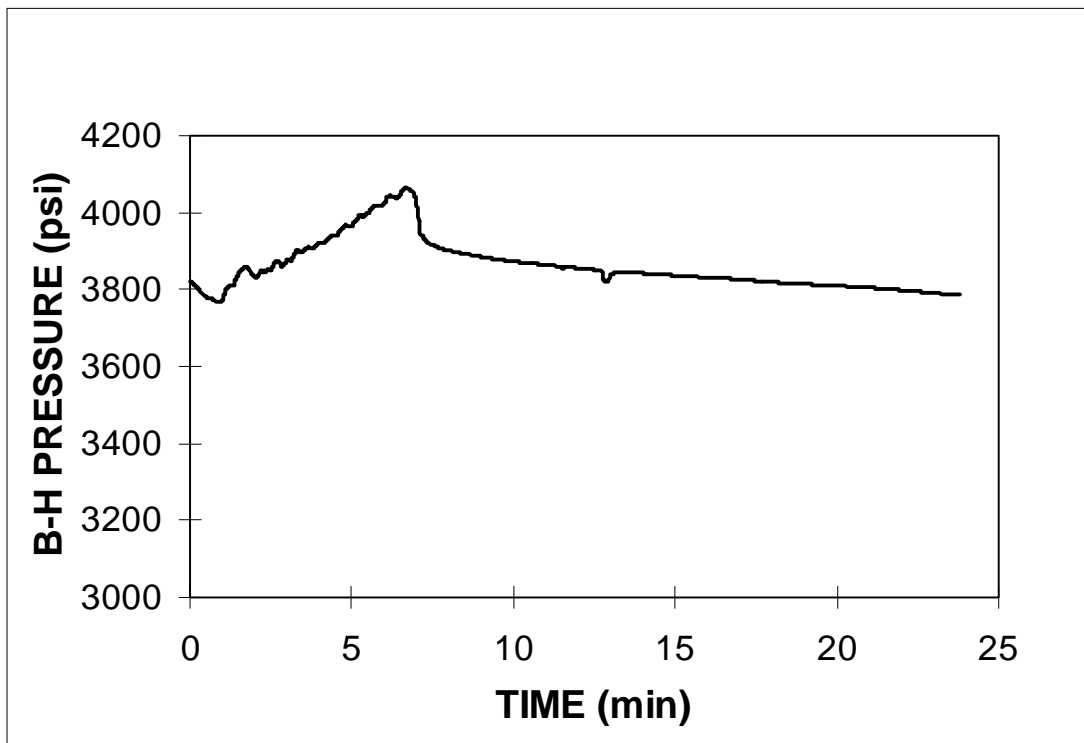


Figure 12. Pressure data for 1C injection.

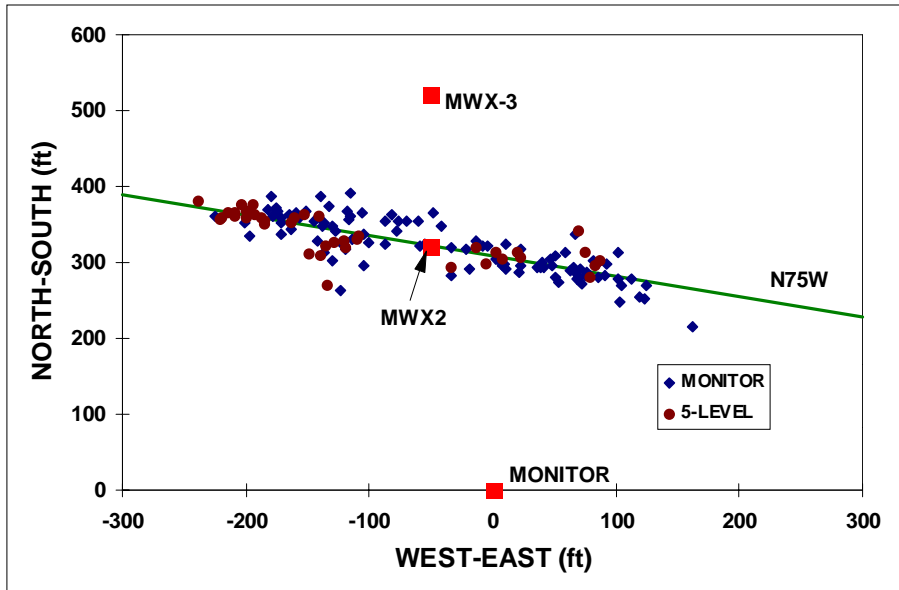


Figure 13. Plan view of all injection 1C microseisms

Figure 14 shows a plan view of these same data. The fracture appears to have grown upward about 20-30 ft, particularly on the west wing, while it has generally avoided the lower part of the C sandstone. The fracture shape is also relatively symmetric.

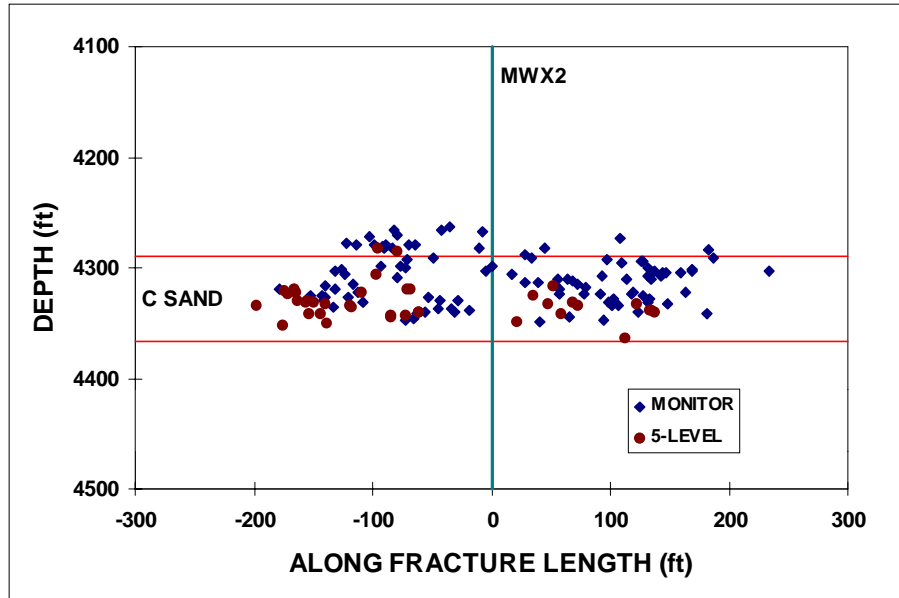


Figure 14. Side view of all injection 1C microseisms

Additional information about hydraulic-fracture mechanisms can often be gleaned from observing the time-dependent growth of the fracture. Figure 15 shows a plan view of the microseisms recorded after 5 minutes, which is the point where shut-in occurred. At this time there are relatively few microseisms and they only show fracture growth out to 130 ft on each wing. The side view, shown in Figure 16, indicates that initial growth was within the center of the C sandstone and above the C sandstone on the west wing.

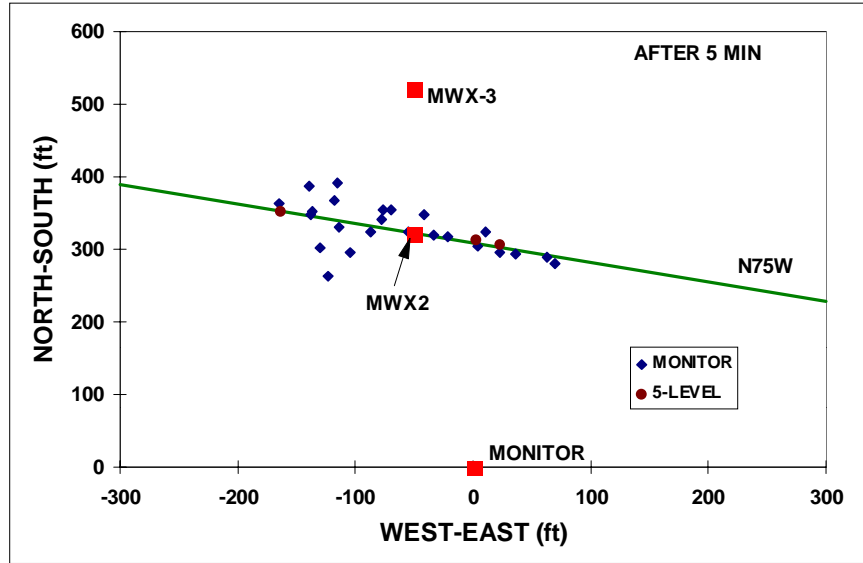


Figure 15. Plan view of injection 1C microseisms recorded after 5 minutes (shut in)

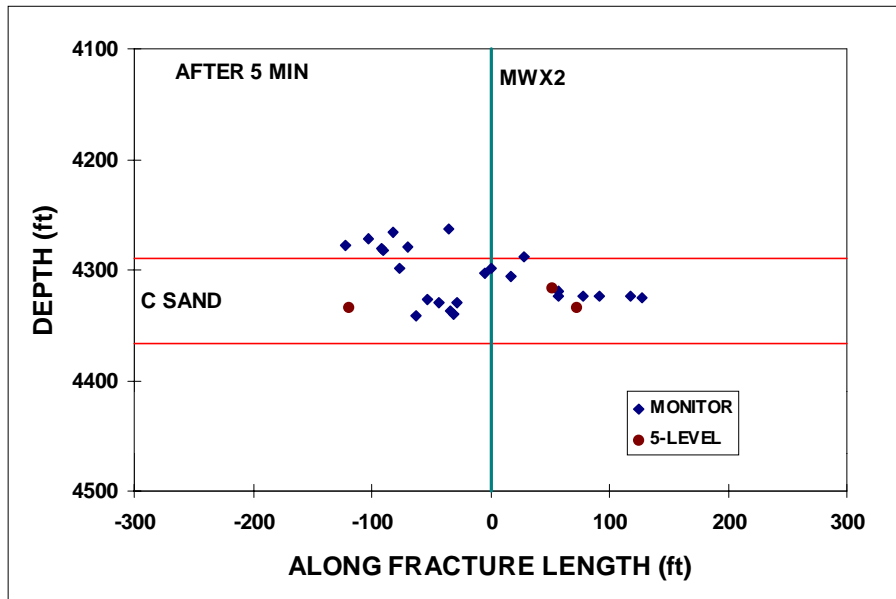


Figure 16. Side view of injection 1C microseisms recorded after 5 minutes (shut in)

The corresponding microseismic plan and side views after 10 minutes are shown in Figures 17 and 18. At this time, the fracture has reached its full length extension on the east wing and most of its final length on the west wing. The fracture height has attained its final value by this time. Clearly, the fracture has continued growing for several minutes after injection terminated, but this growth is not surprising given the relatively small leakoff of the viscous crosslinked gel in the low permeability sandstone.

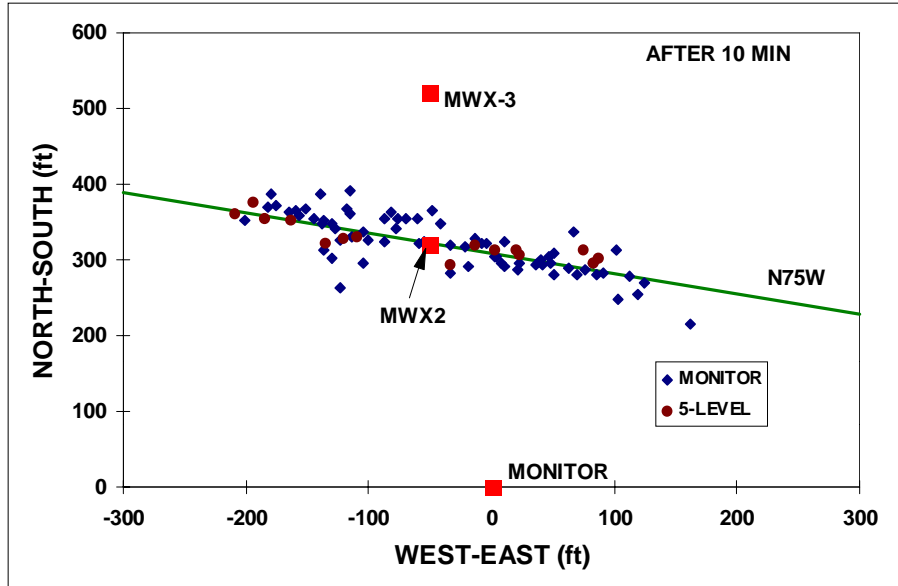


Figure 17. Plan view of injection 1C microseisms recorded after 10 minutes

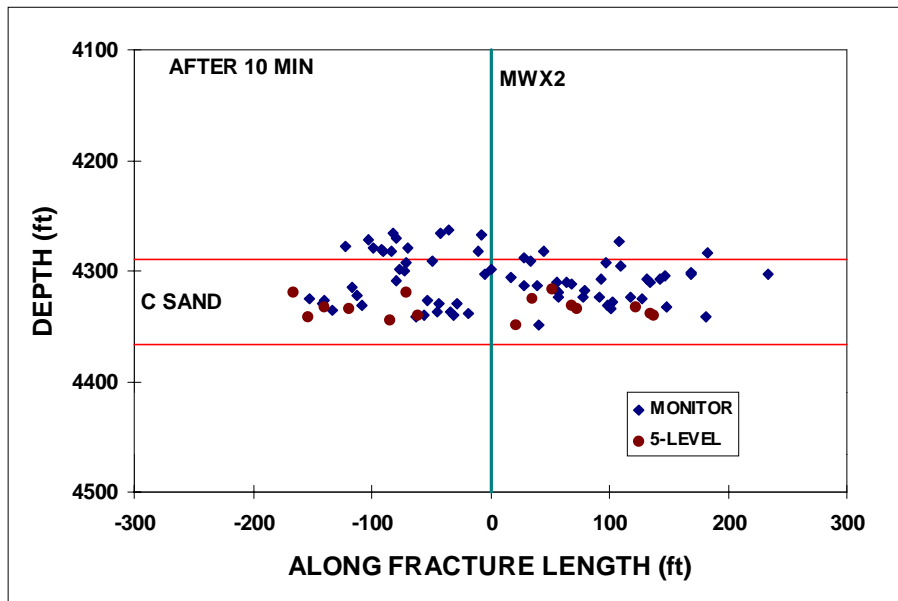


Figure 18. Side view of injection 1C microseisms recorded after 10 minutes

Figures 19 and 20 show the plan and side views of the microseismic results after 20 minutes. There are considerably more microseisms, but none that appear to be associated with fracture extension (except possibly a few on the far west wing). Thus, it is likely that most of the microseisms that occurred from 10 to 20 minutes after the start of the test are associated with leakoff into the natural fractures and other planes of weakness.

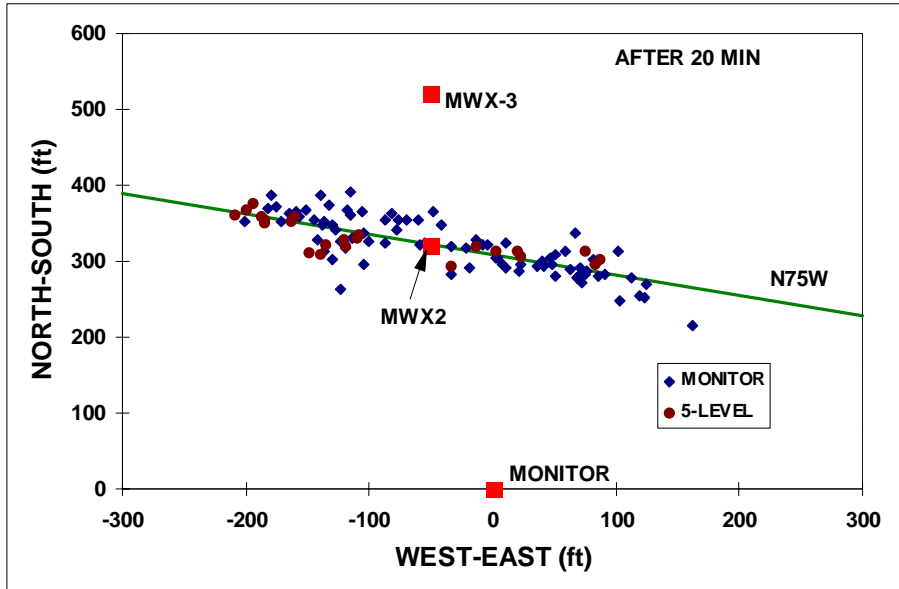


Figure 19. Plan view of injection 1C microseisms recorded after 20 minutes

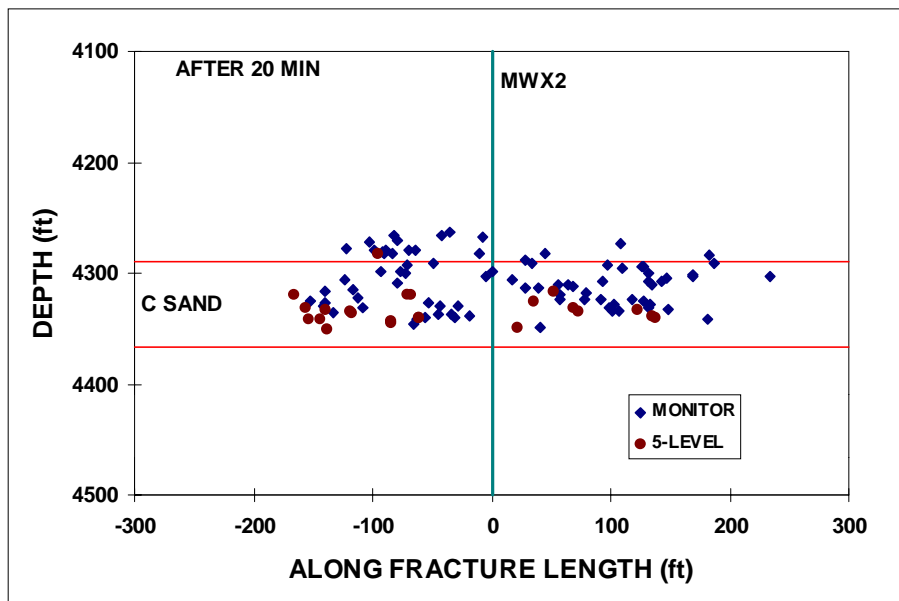


Figure 20. Side view of injection 1C microseisms recorded after 20 minutes

Figures 21 and 22 show the plan and side views of the microseisms obtained after 30 minutes. The only difference in the geometry might be a slight amount of length extension in the center part of the C sandstone on the west wing. In general the fracture geometry is very similar to that seen at the end of the test (53 minutes after injection started), as can be seen by comparing these results with the results shown in Figures 13 and 14.

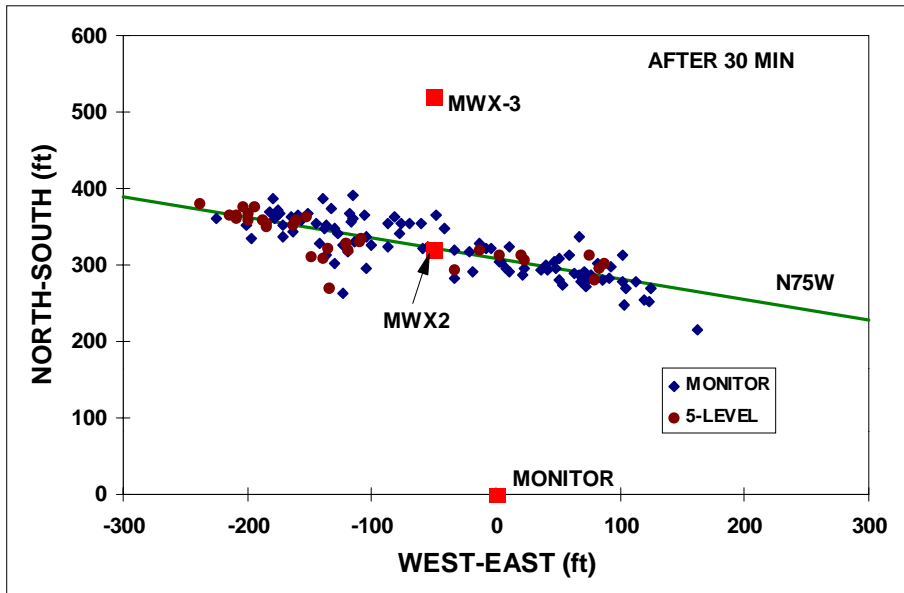


Figure 21. Plan view of injection 1C microseisms recorded after 30 minutes

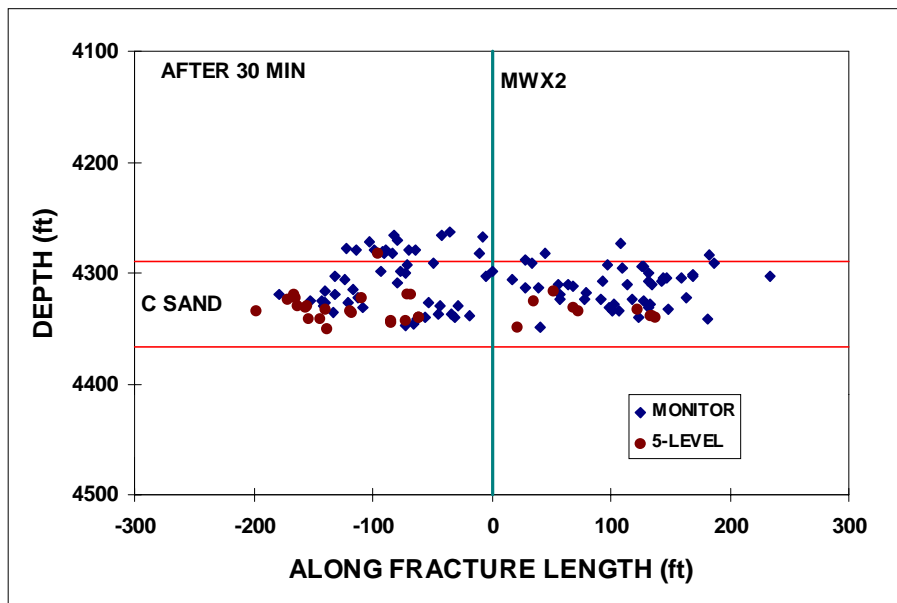


Figure 22. Side view of injection 1C microseisms recorded after 30 minutes

There is no additional interpretation of the fracturing behavior as this was a very short pump and the first one in this sandstone interval. The fracture appears well behaved and the slight upward growth is not inconsistent with the 1000 psi net treatment pressure observed during this injection.

8.3.5 Injection 2C microseismic results

Injection 2C, which was conducted on August 8, 1996, was designed to be a linear-gel minifrac which would approach the intersection well without hitting it. The design volume was 250 bbl at a design rate of 20 bpm. However, recognizing that fracture growth is very uncertain in these complex fluvial geometries, it was decided that at the first sign of pressure increase in the intersection well, the treatment would be terminated.

Such a pressure increase was observed after pumping 130 bbl and the treatment was terminated with a total injected volume of 136 bbl at 22 bpm. This intersection then provided a validation point for the microseismic results, as it defined a time when the fracture length was known with great accuracy. The pressure data for this injection is shown in Figure 23. The injection included a step-up pump at the beginning of the injection and then a quick step-down and shut-in for near-wellbore pressure-drop estimates. Finally, injection started again at about 9 minutes and continued until a pressure increase was observed in IW-1C. The maximum net pressure for this injection was about 900 psi.

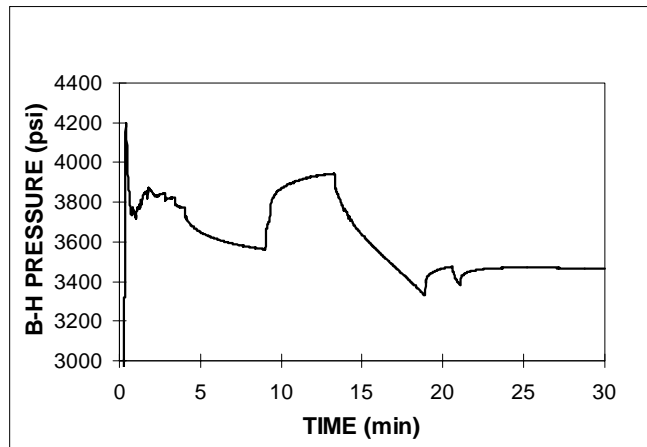


Figure 23. Pressure data for 2C injection

Figures 24 and 25 show the plan and side views of all of the microseisms recorded during the 2C injection. The full 136 bbl injection results in an approximately N74°W azimuth with an east wing length of at least 400 ft and a west wing that is slightly less. On both wings, the fracture appears to avoid the lower part of the C sandstone. There is no upward growth on the west wing of the fracture, but the east wing shows upward height growth starting about 150 ft east of the wellbore.

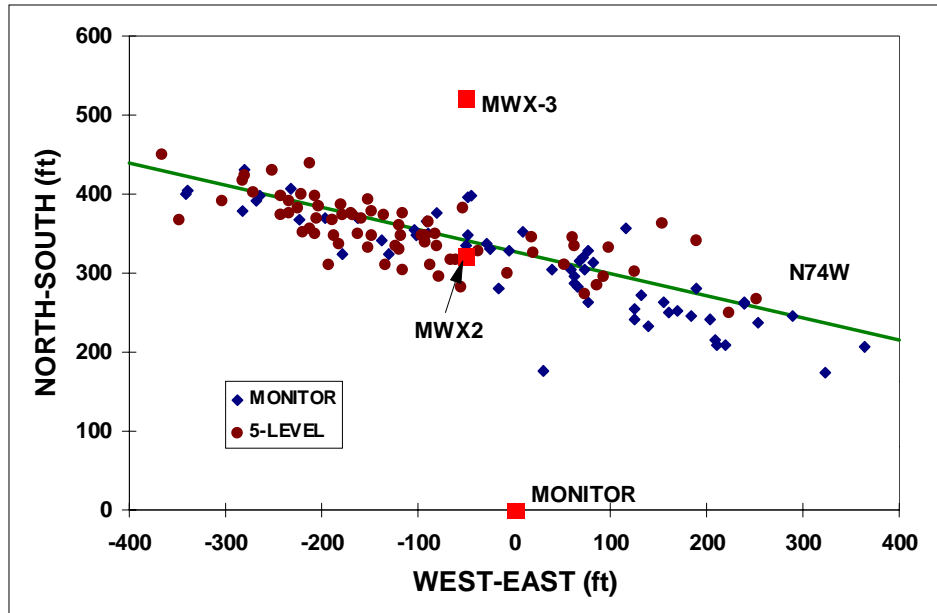


Figure 24. Plan view of all injection 2C microseisms.

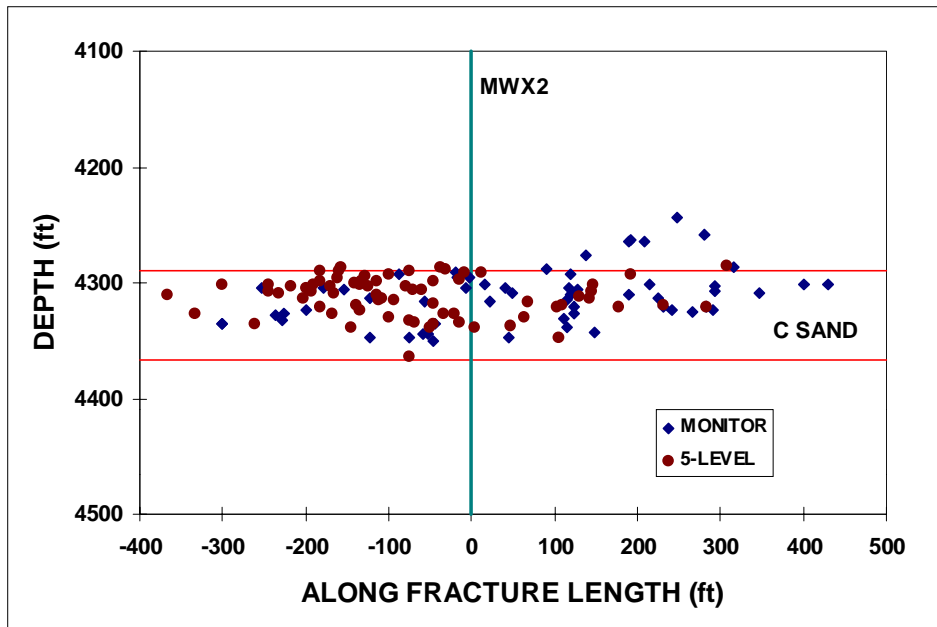


Figure 25. Side view of all injection 2C microseisms.

Figures 26 and 27 show the microseisms that have been obtained after 5 minutes (60 bbl injected) of pumping. The initial growth is somewhat asymmetric with a west wing length of 250 ft at this time and an east wing length of 150 ft. No microseisms are observed in the very bottom of the C sandstone and no height growth is yet observed.

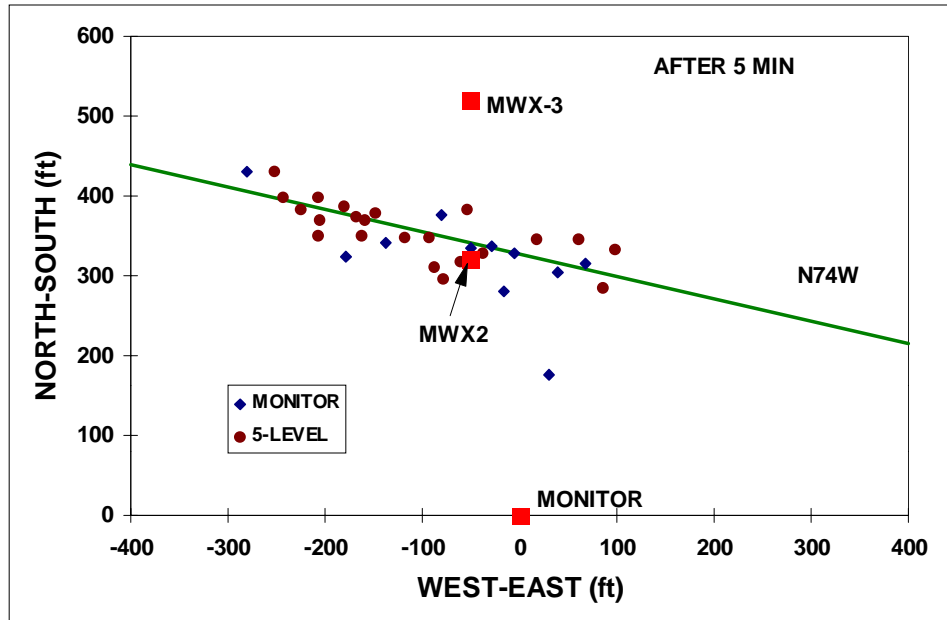


Figure 26. Plan view of injection 2C microseisms recorded after 5 minutes of testing.

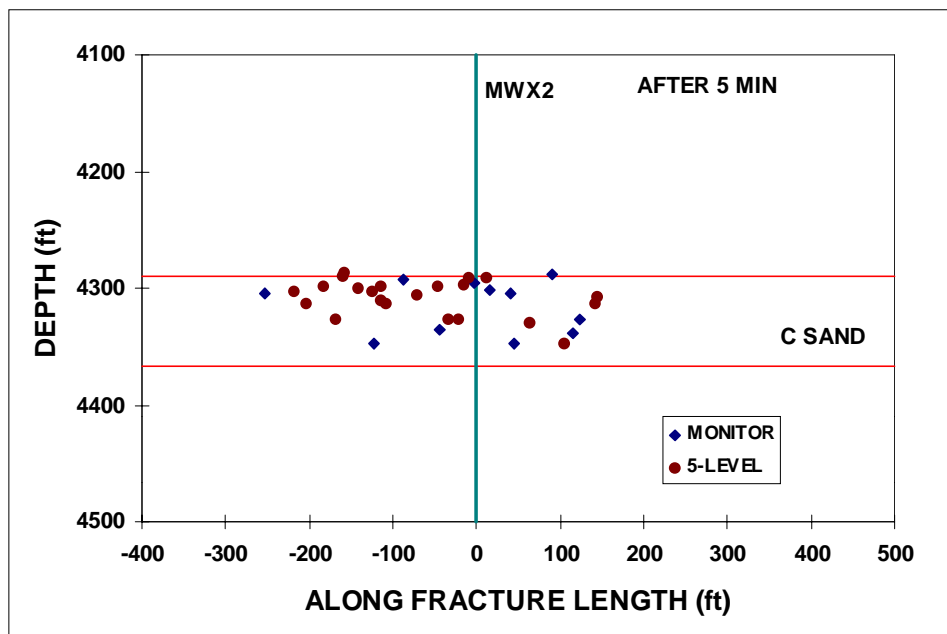


Figure 27. Side view of injection 2C microseisms recorded after 5 minutes of testing.

Figures 28 and 29 show the plan view and side views of the microseisms recorded after 10 minutes. At this time, pumping had resumed after a short shut in for near-wellbore pressure drop estimates. Since the time pumping restarted, it appears that all the new fracture growth was on the east wing, giving a very symmetric shape with 250 ft wing lengths. No evidence of height growth has yet been observed.

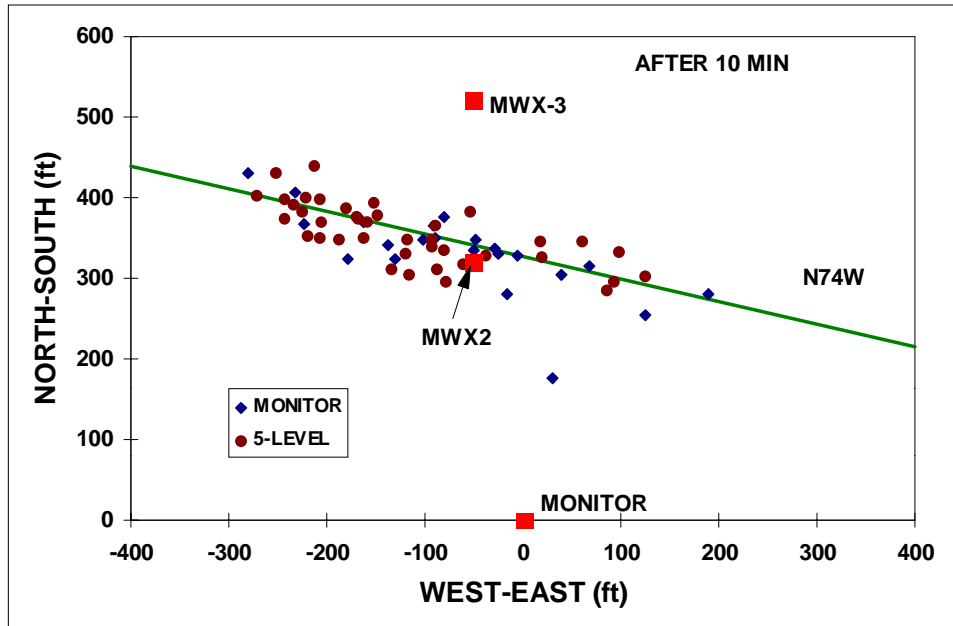


Figure 28. Plan view of injection 2C microseisms recorded after 10 minutes of testing.

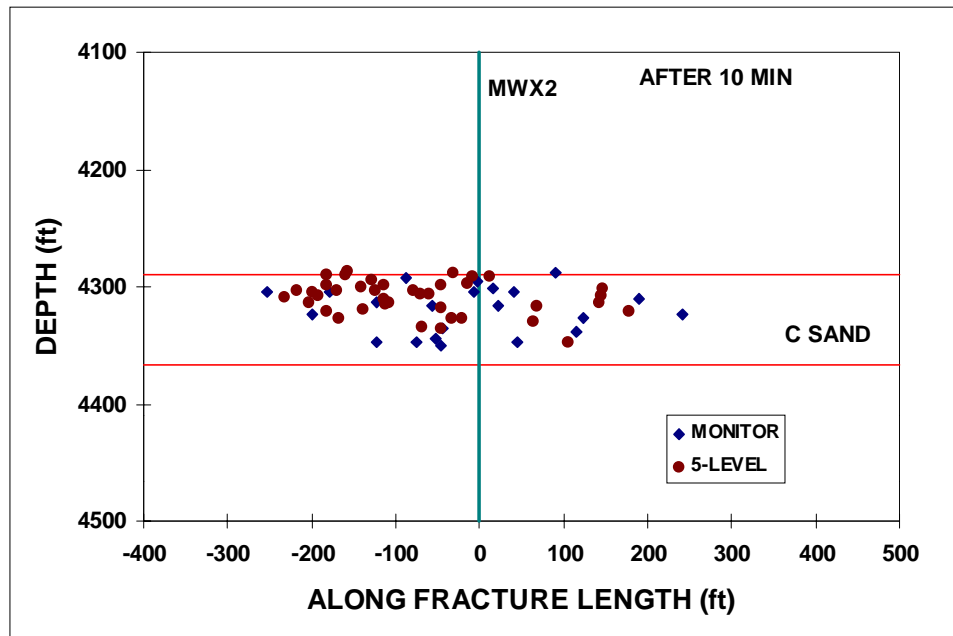


Figure 29. Side view of injection 2C microseisms recorded after 10 minutes of testing.

Figures 30 and 31 show the most important microseismic result associated with the C sandstone experiments. They give the microseismic fracture geometry at the time that pressure was observed in the intersection well and the fracture length was approximately 300 ft (the exact distance depends on the exact azimuth of the fracture). It can be clearly seen in Figure 31 that the microseismic length is also 300 ft on the east wing, thus validating the accuracy of the microseismic length results. In this test, the west wing length is also nearly 300 ft. It is also about this time that upward fracture growth on the east wing began to occur.

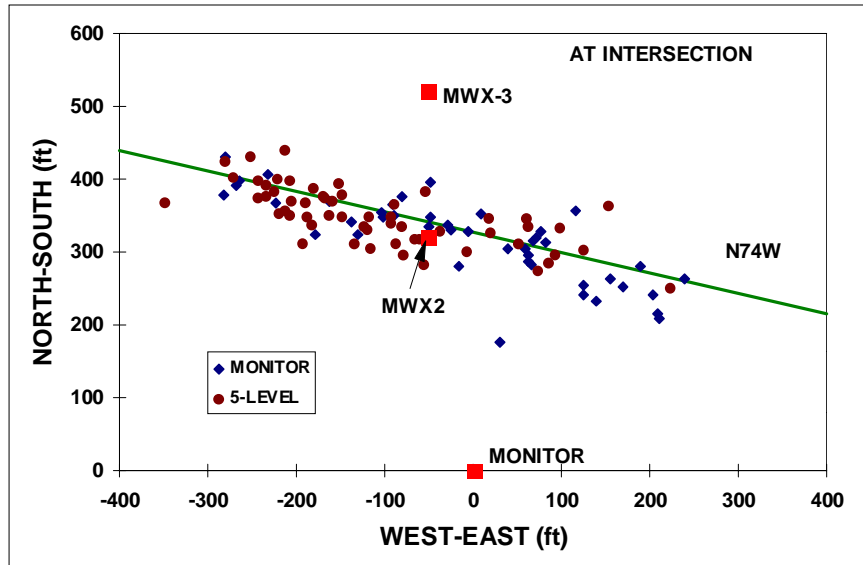


Figure 30. Plan view of injection 2C microseisms at the time of intersection of IW-1C.

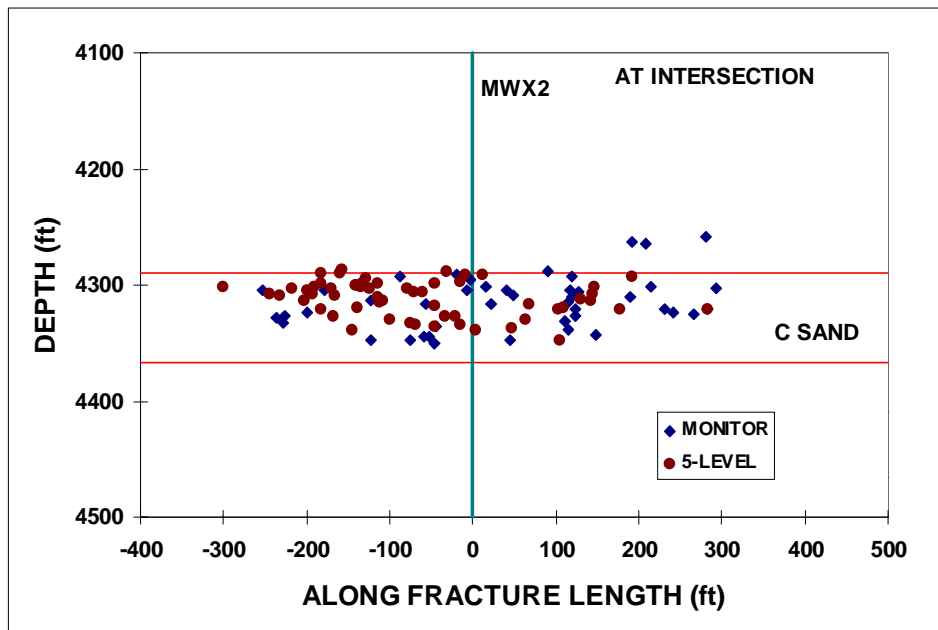


Figure 31. Side view of injection 2C microseisms at the time of intersection of IW-1C.

As noted previously, these 2C microseismic results are the most important aspect of this entire test, as the complete validation of the accuracy of the microseismic results has been obtained. However, some interesting results with respect to fracture growth can also be seen in these data. The avoidance of the lower part of the C sandstone was unexpected and is probably related to either the shale break seen in the lower part of the C sandstone or due to a higher stress in the lower C sandstone. There is support for a dual stress regime in the C sandstone, as the current closure stress measurements indicate a stress of 3050 psi in the interval that is fracturing, while a previous stress measurement in the lower C sandstone indicated a stress of 3350 ± 75 psi (Warpinski and Teufel, 1989). The fracture growth upward on the east wing is more difficult to explain, as height growth would have been expected near the wellbore where the pressure is the highest. One possible explanation is the existence of additional sandstone

units at the top of the C sandstone on the west wing. Such an interpretation is supported by the cross-well seismic survey, which indicated that the C sandstone shifted upward in the section between MWX-2 and the monitor well. The p-wave and s-wave tomograms of the survey are shown in Figures 32 and 33, with the left side of the figure being MWX-3 and the right side being the monitor well. MWX-2 is left of center at about 200 ft and not shown as a discrete line, although it can be seen faintly in the data. The whiter regions indicate the higher velocities of the sandstone, and it is clear that about 150 ft south of MWX-2 there is an upward shift in both the p-wave and s-wave representation of the sandstone. Since this upper sand unit does not extend north into the treatment-well region, it is likely that it extends east-west and may be the reason for the upward fracture growth. Basically, it suggests that the fracture is merely following the sandstone channel and there is no out-of-zone growth.

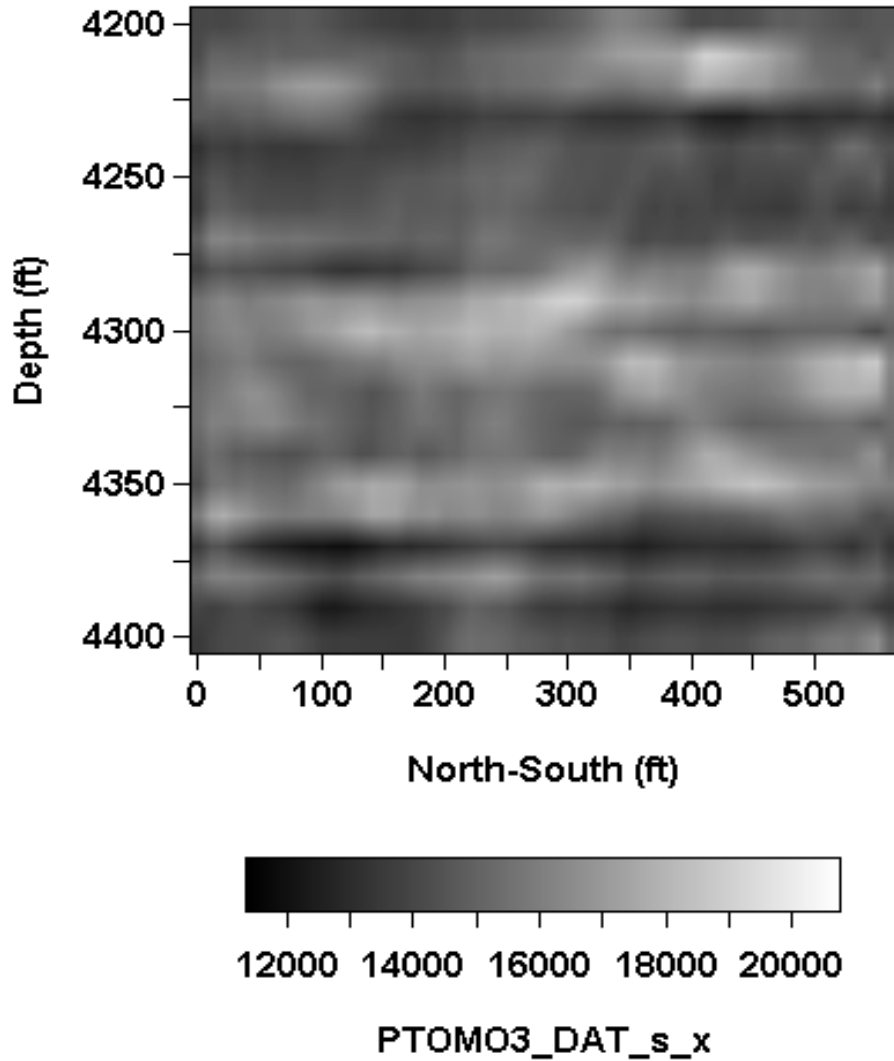


Figure 32. P-wave tomogram of C sandstone region showing possible additional sandstone

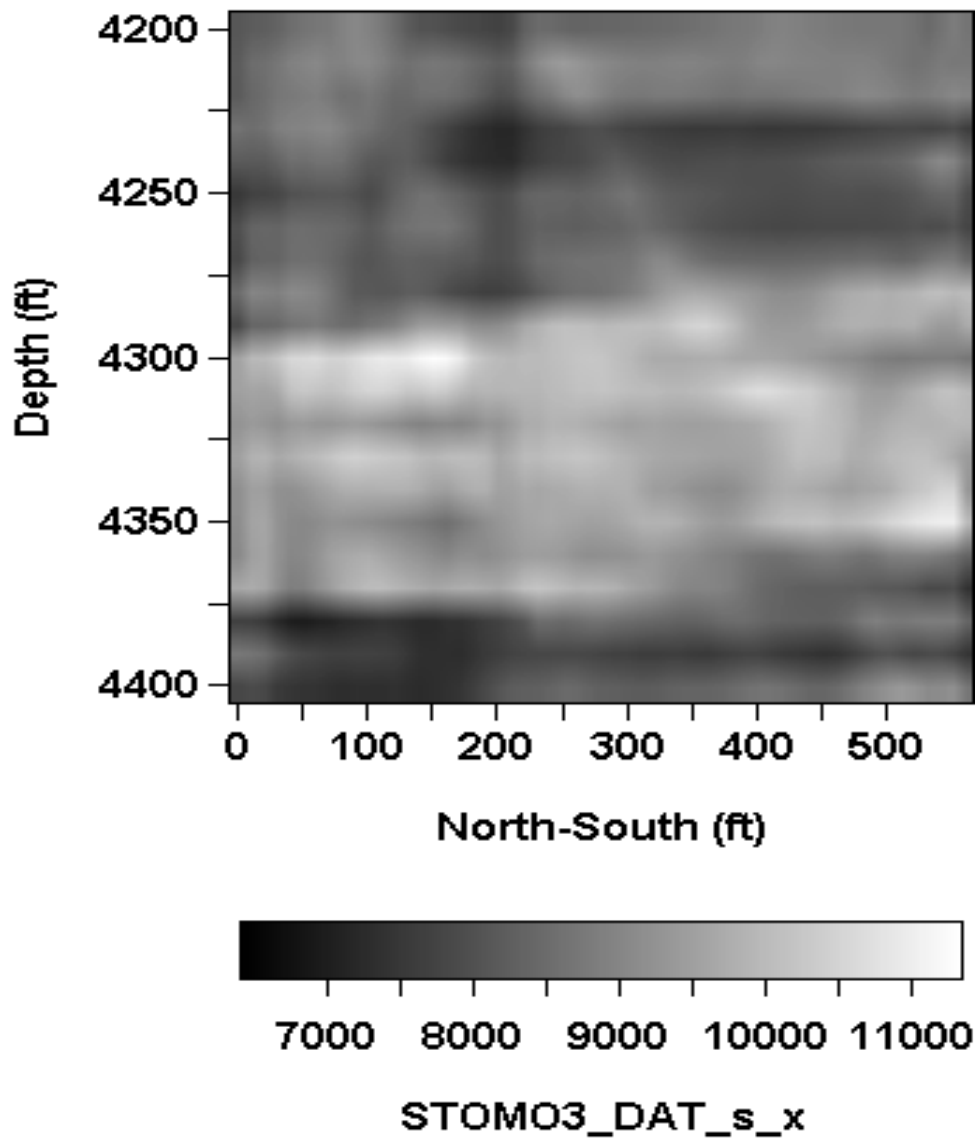


Figure 33. S-wave tomogram of C sandstone region showing possible additional sandstone

It was also learned afterwards that the pressure communication between MWX-2 and the well IW-1C was non-existent and it was not even certain that the well had actually been intersected by the hydraulic fracture. No fractures were observed in the intersection well after an FMS log and the microseisms indicated that the fracture might have been above the intersection well. Thus the pressure response could have been due to stressing of the wellbore as the fracture passed close by, rather than a direct pressure communication. An alternate interpretation is that the fracture intersected the IW-1C well, but through some tortuous path in the shaley layers below the C sandstone or in some other fashion. There is insufficient evidence to clearly define what occurred in this test.

8.3.6 Injection 3C microseismic results

Injection 3C, which was conducted on August 21, 1996, was a repeat of injection 2C, except that a full 250 bbl was injected. It was hoped that the uncertainties associated with the 2C injection could be remedied with a larger linear-gel injection that would more adequately intersect the IW-1C well. Figure 34 shows the pressure response during the test. Step-up, step-down, and shut-in periods were conducted during this injection, resulting in the complex pressure results. Most of the volume was injected in the latter part of the test at a rate of 24 bpm and a maximum net pressure of about 950 psi.

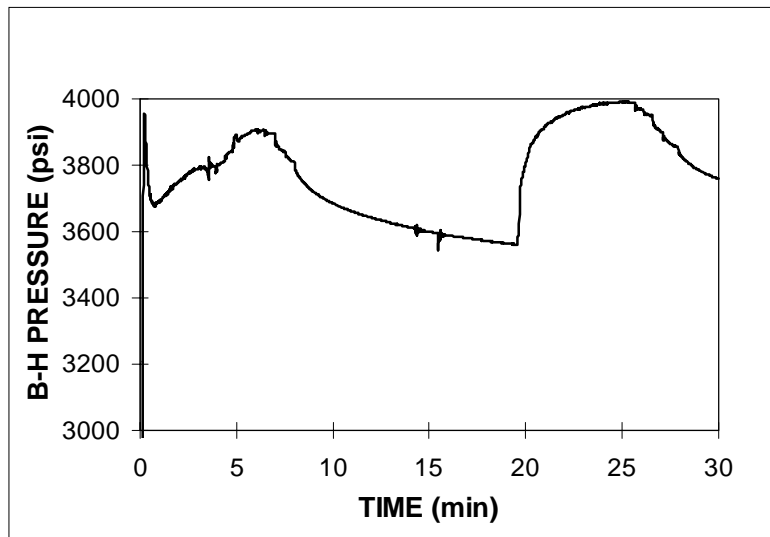


Figure 34. Pressure data for 3C injection.

Microseismic results of injection 3C are shown in plan and side view in Figures 35 and 36. This fracture has an injected volume of only 250 bbl and a fairly high leakoff because it is a linear gel, yet the fracture lengths are almost 500 ft on the east wing and more than 400 ft on the west wing. The azimuth through all three initial injections have been N74°W or N75°W. This fracture may have finally broken down into the lower part of the C sandstone and also shows some slight evidence of height growth near the wellbore. The upward growth on the far east wing, which was first seen in the 2C injection, is also obvious in this test.

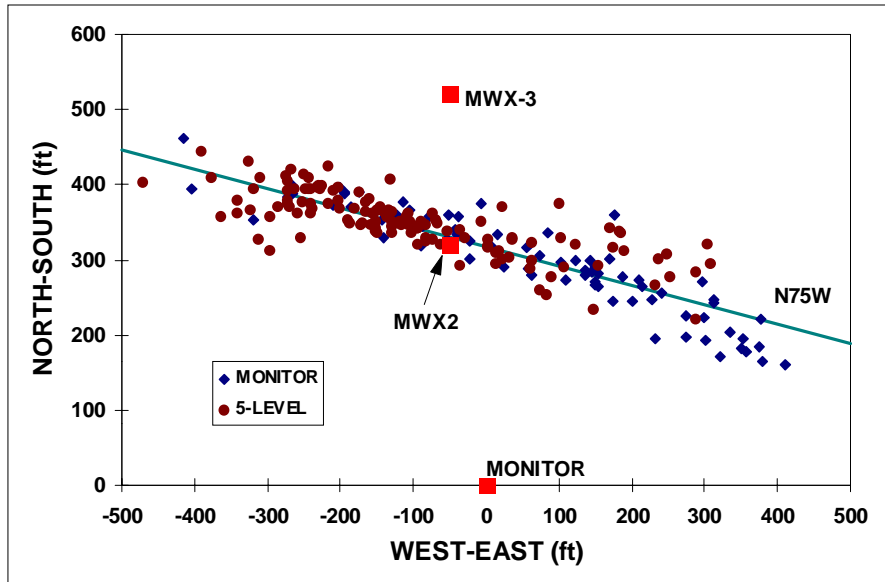


Figure 35. Plan view of all injection 3C microseisms

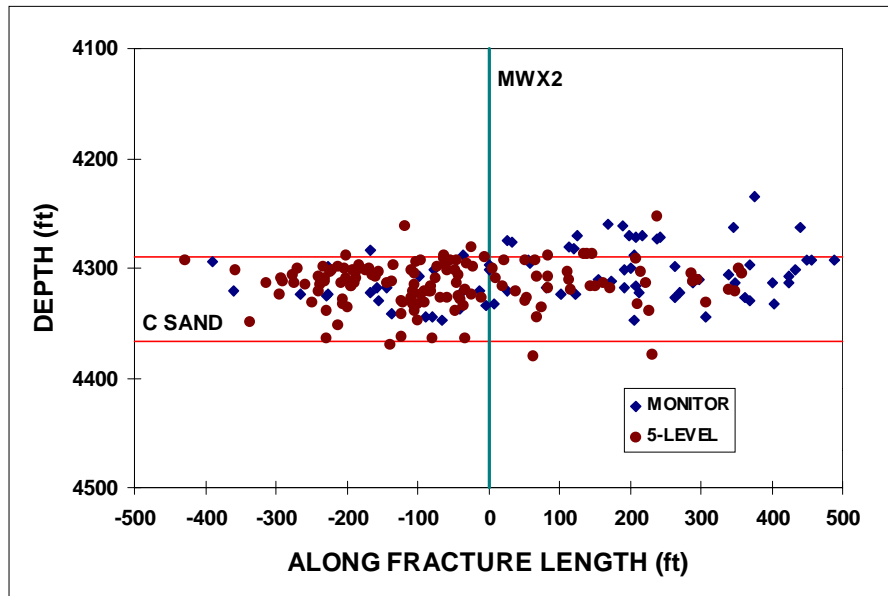


Figure 36. Side view of all injection 3C microseisms.

The microseisms recorded after 10 minutes of testing are shown in plan and side views in Figures 37 and 38. It was at this time that a slow rise in pressure was first observed in the intersection well, indicating the fracture was likely to be close to IW-1C. While sparse, the microseisms also indicate the fracture grew rapidly out to about 300 ft length on the east wing (thus the reason for the pressure increase in IW-1C) and about 250 ft length on the west wing. The fracture again initiates in the upper part of the C sandstone and shows a small possibility of slight upward extension.

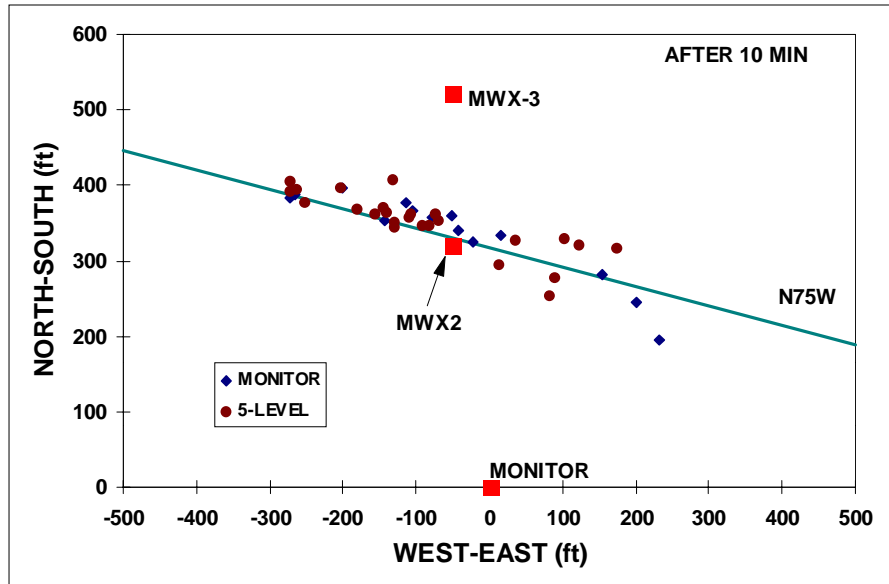


Figure 37. Plan view of injection 3C microseisms after 10 minutes of testing.

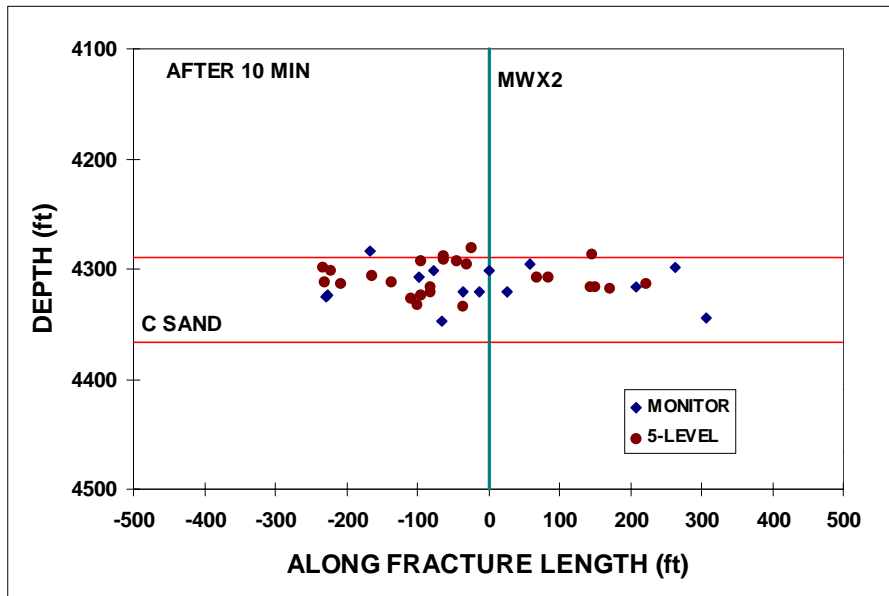


Figure 38. Side view of injection 3C microseisms after 10 minutes of testing.

After 20 minutes of testing, which is just after pumping resumed following the shut-in period, the plan and side views of the injection are shown in Figures 39 and 40. Most of the microseisms during this period were fill-in events and little evidence of additional extension is evident.

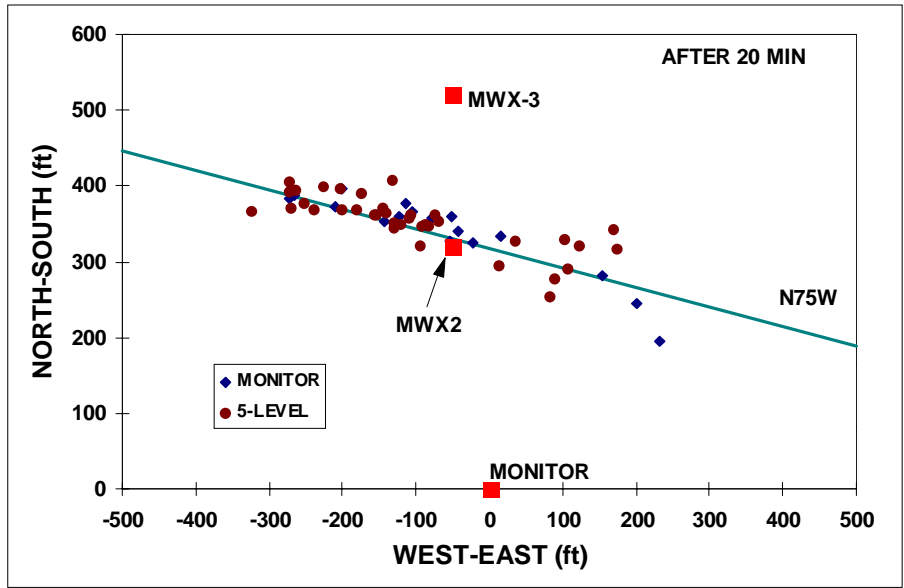


Figure 39. Plan view of injection 3C microseisms after 20 minutes of testing.

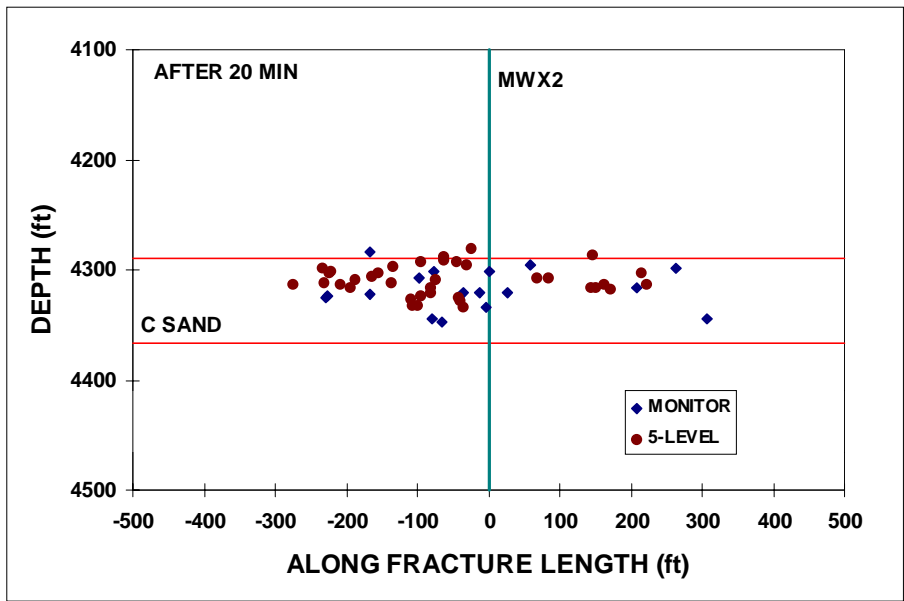


Figure 40. Side view of injection 3C microseisms after 20 minutes of testing.

The plan and side views of the recorded microseisms after 30 minutes of testing are shown in Figures 41 and 42. This time is just after shut-in following a step-down test. Fracture length has quickly grown to nearly its full extent and considerable upward growth has occurred on the east wing during this time period.

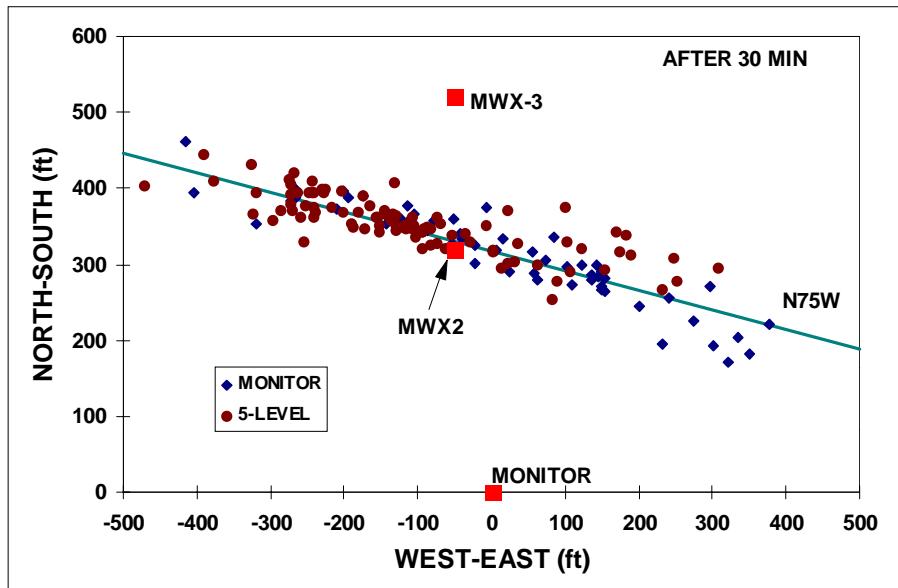


Figure 41. Plan view of injection 3C microseisms after 30 minutes of testing.

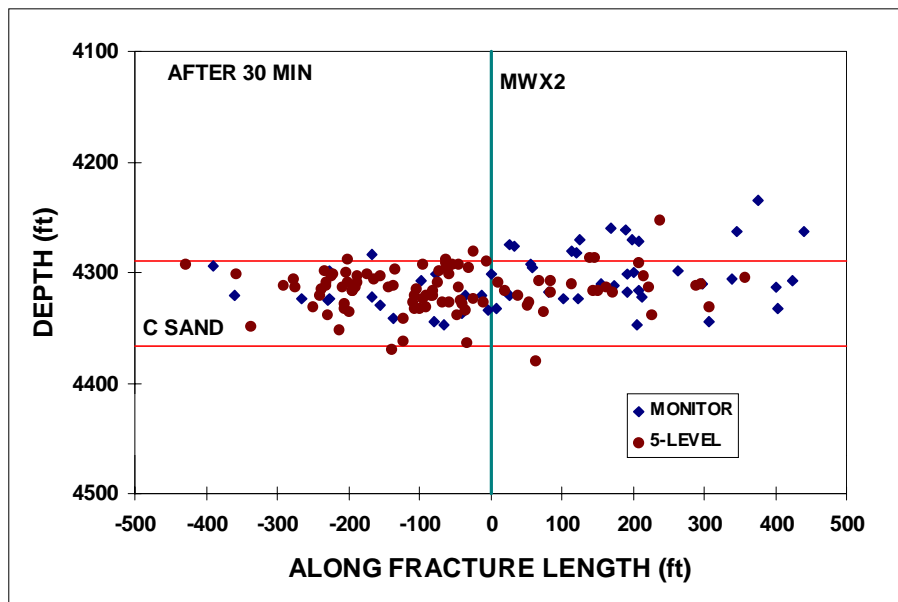


Figure 42. Side view of injection 3C microseisms after 30 minutes of testing.

Figures 43 and 44 show plan and side views of the microseisms recorded after 40 minutes of testing, which corresponds to about 10 minutes after shut in. There have been considerably more microseisms since shut in, but no evidence of additional fracture growth.

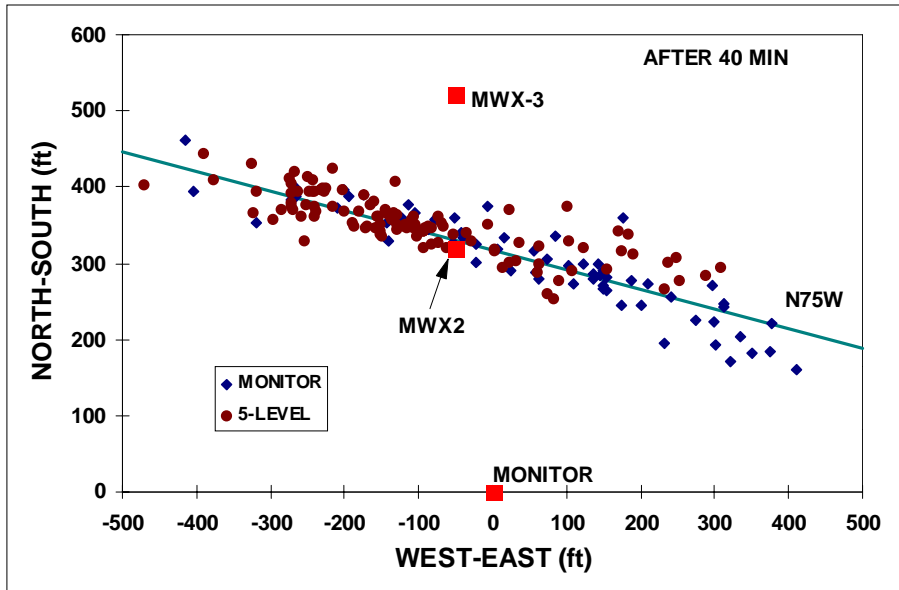


Figure 43. Plan view of injection 3C microseisms after 40 minutes of testing.

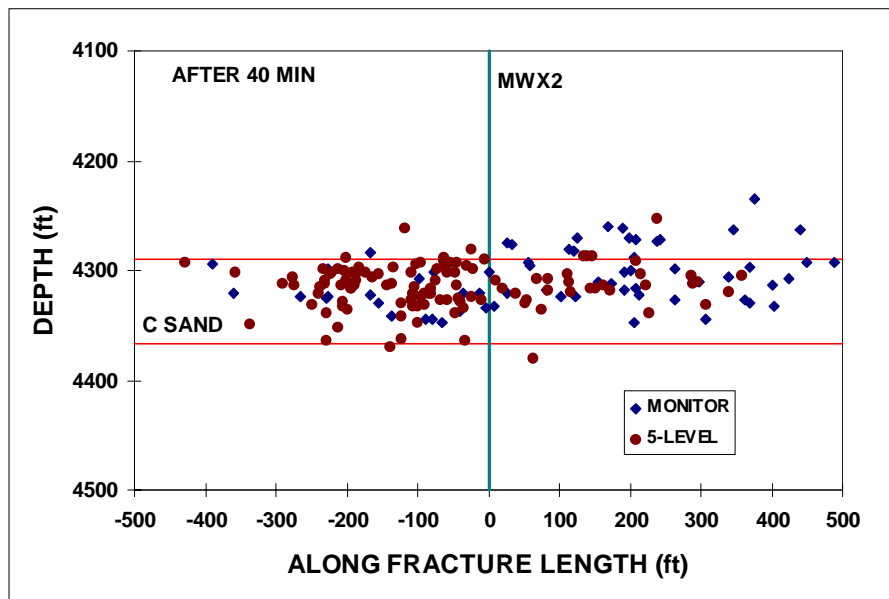


Figure 44. Side view of injection 3C microseisms after 40 minutes of testing.

This injection showed a fracture that rapidly grew in length and exhibited some upward growth as the net pressure approached 1000 psi. The intersection with IW-1C occurred relatively early in the treatment, but, as in injection 2C, it was not a totally clear connection. The microseisms again suggest that the hydraulic fracture may have been above the intersection well, since little microseismic activity occurred in the lower C sandstone on the east wing. This test also showed the rising fracture behavior on the east wing, but it is obscured somewhat by the increased height growth near the wellbore.

8.3.7 Injection 4C microseismic results.

Injection 4C, conducted on November 22, 1996, was a dual objective test. Approximately 1000 bbl of 40# crosslinked gel were injected into the C sandstone at about 40 bpm in order to test the possibility of obtaining treatment well diagnostics and to give one final attempt at obtaining a clear intersection of IW-1C. To test the treatment well diagnostics, a four-level seismic array was placed in the treatment well, straddled over the C sandstone. Unfortunately, during initial injection of water in the casing, the turbulence of the thin fluid induced sufficient vibration to loosen a locking nut on the fiber-optic cable head, causing a break in the copper and fiber-optic lines (but the cable armor remained connected and there was not a complete disconnect of the tool string). Thus, no treatment well diagnostics were obtained during this test and a lesson was learned regarding placement of treatment-well strings during pumping.

After the loss of the treatment-well string, the remaining diagnostics were the monitor-well receivers, which functioned very well during this test. The injection consisted of the bullnosing of 132 bbl of KCl water, which was in the casing originally, followed by the injection of the crosslinked gel in two stages, separated by a 15 minute shut-in period for leakoff and near-wellbore analyses. Figure 45 shows the pressure data obtained during this injection. The initial pressure rise (0-30 min) corresponds to the bullnosing of water into the formation, followed by a long shut-in. Injection of the gel starts at about 95 minutes, with the gel shut-in occurring at about 110 minutes. Gel injection resumes at about 125 minutes, but at first the gel would not move and surface pressures reached their maximum allowable at rates of only 1-2 bpm. Finally the fluid started to move and rates were eventually built to their design values. However, at the point where the gel began moving and fracturing clearly restarted, there was a tremendous burst of microseismic activity. Net pressures varied considerably during the treatment, but an average net pressure after fracturing resumed following the shut-in period is roughly 1200 psi.

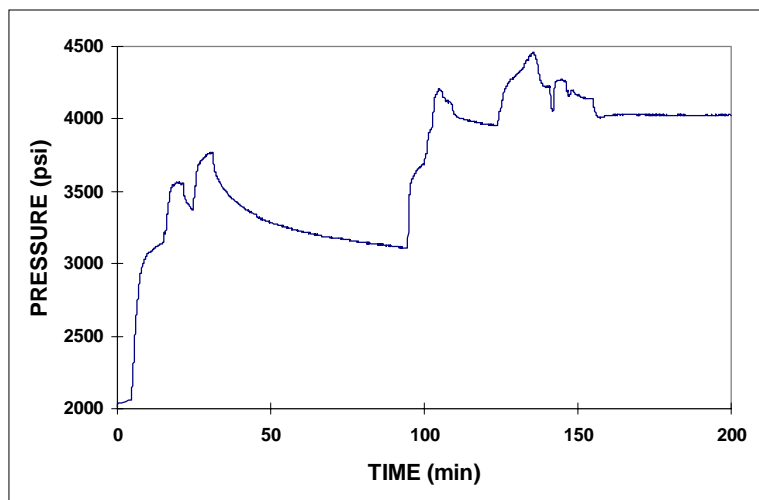


Figure 45. Injection 4C pressure data

All of the microseisms from the 4C injection are shown in plan view and side in Figures 46 and 47, respectively. Fracture 4C is clearly an asymmetric fracture with considerable height growth. The east wing length is 600-700 ft while the west wing is only about 400 ft. Fracture growth upward is 60-80 ft, depending on the location, while growth downward is about 50 ft, but only on the west wing.

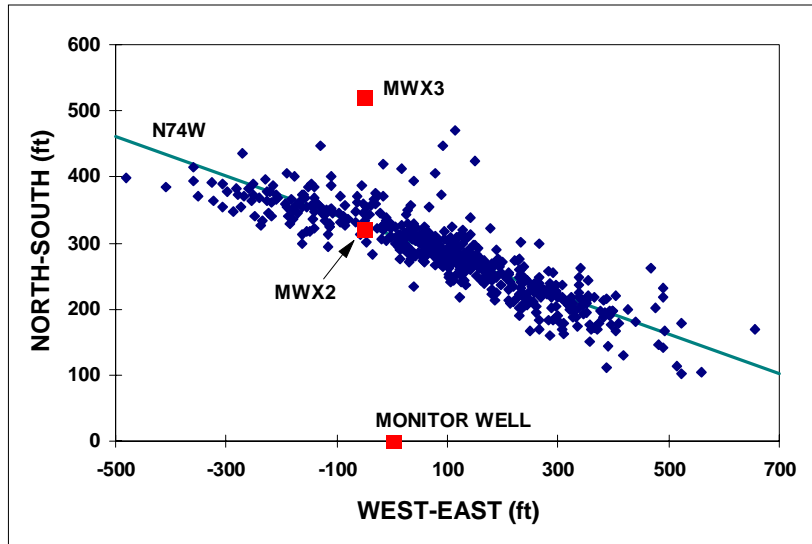


Figure 46. Plan view of all injection 4C microseisms.

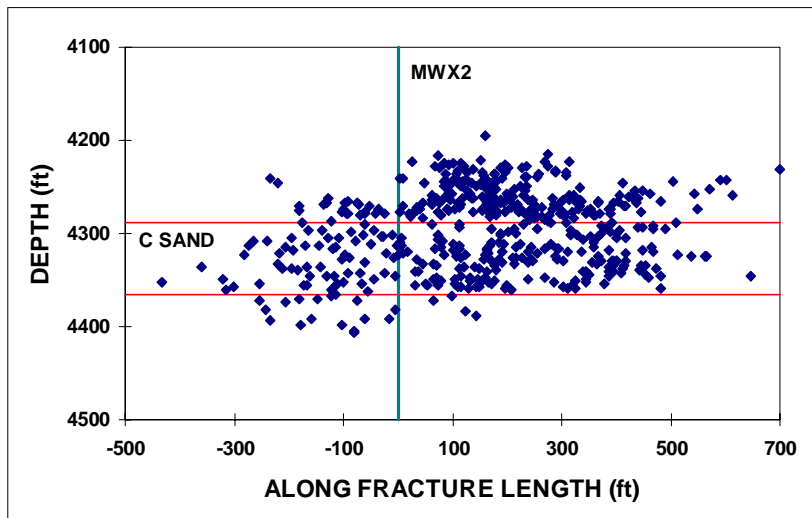


Figure 47. Side view of all injection 4C microseisms.

The initial microseisms that were detected during the injection of the KCl water in the casing string are shown in Figures 48 and 49. Only a few microseisms were detected during this period, but they indicate that the fracture grew rapidly to a length of approximately 300 ft. During this injection, a slow pressure rise was noted in the IW-1C well, confirming that the fracture had grown out to at least 300 ft.

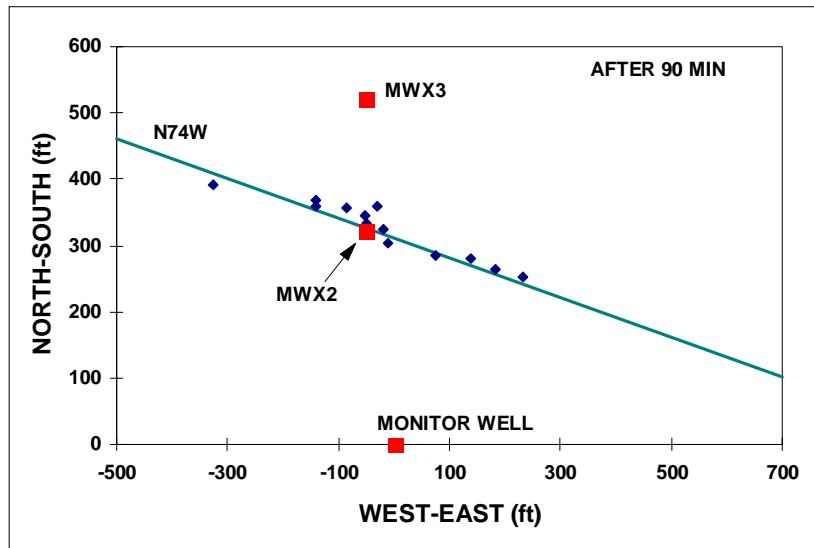


Figure 48. Plan view of injection 4C microseisms recorded after 90 minutes of testing.

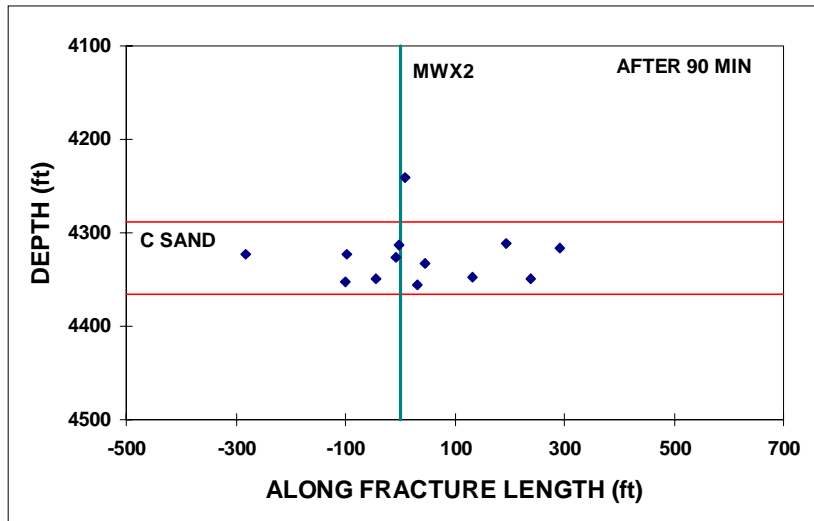


Figure 49. Side view of injection 4C microseisms recorded after 90 minutes of testing.

The microseisms recorded after the first gel injection and shut-in period are shown in Figures 50 and 51. These data indicate that the primary growth of the fracture during this period was upward and downward on the west wing. Some additional length extension also occurred on the east wing. The additional height growth is not surprising, seeing as how the net pressure was greater than 1100 psi during the injection period.

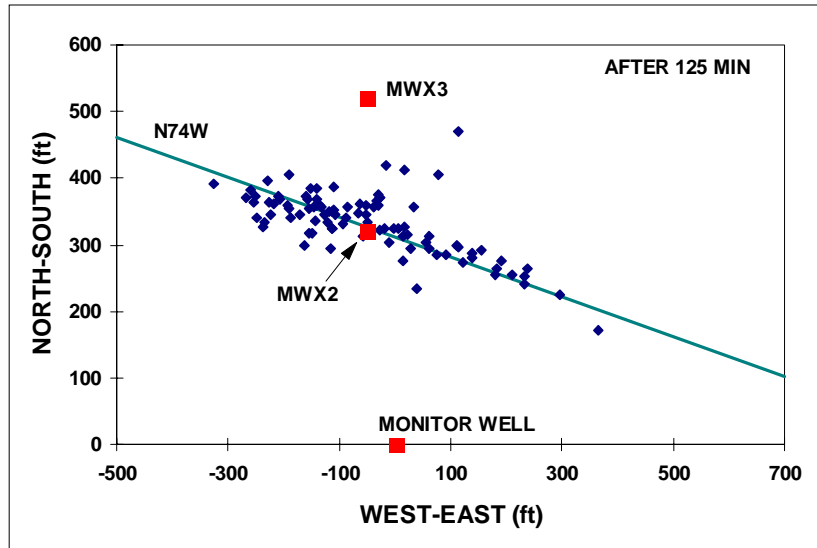


Figure 50. Plan view of injection 4C microseisms recorded after 125 minutes of testing.

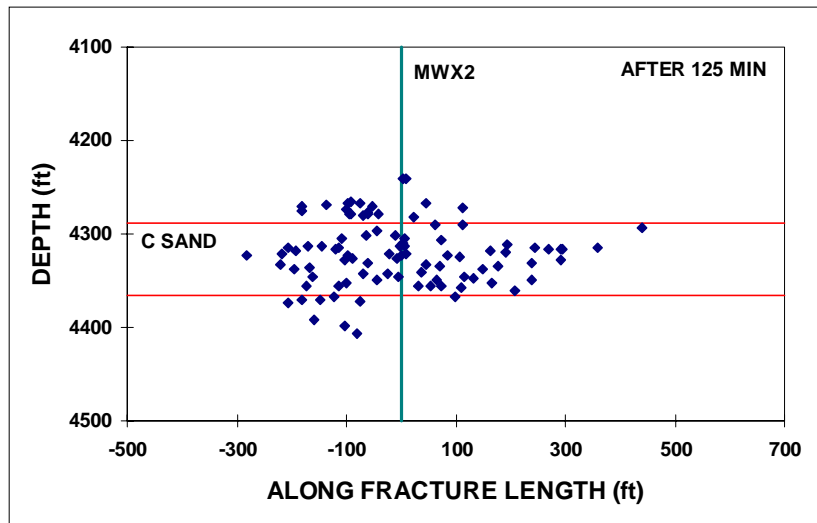


Figure 51. Side view of injection 4C microseisms recorded after 125 minutes of testing.

Figures 52 and 53 show the microseisms that occurred up to the 140 minutes, which is just after the “explosion” of microseisms that were observed when the crosslinked gel finally began moving in the fracture. Fracture growth was predominantly on the east wing, with a fracture length out to 500 ft and a large amount of height growth upward. Microseisms show that IW-1C should have been intersected, and the pressure data showed a very rapid pressure rise up to nearly the treatment well net pressure. Finally, a good connection between the fracture and the intersection well was achieved.

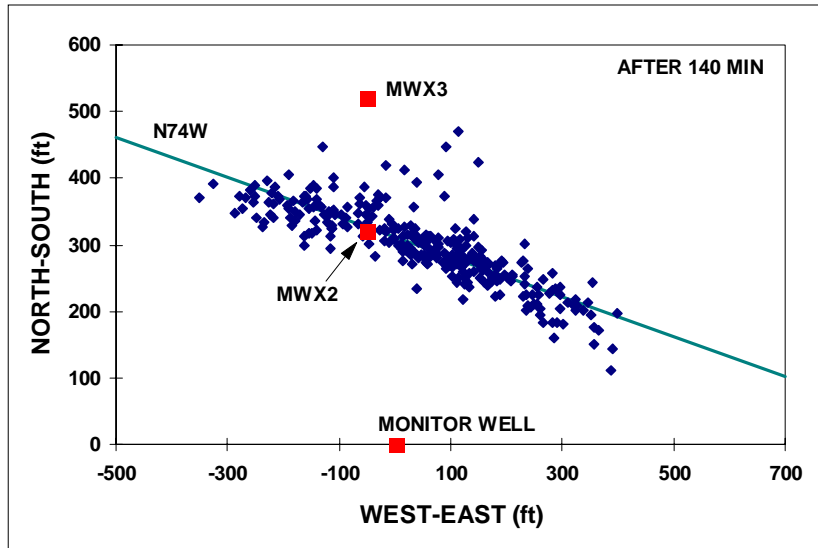


Figure 52. Plan view of injection 4C microseisms recorded after 140 minutes of testing.

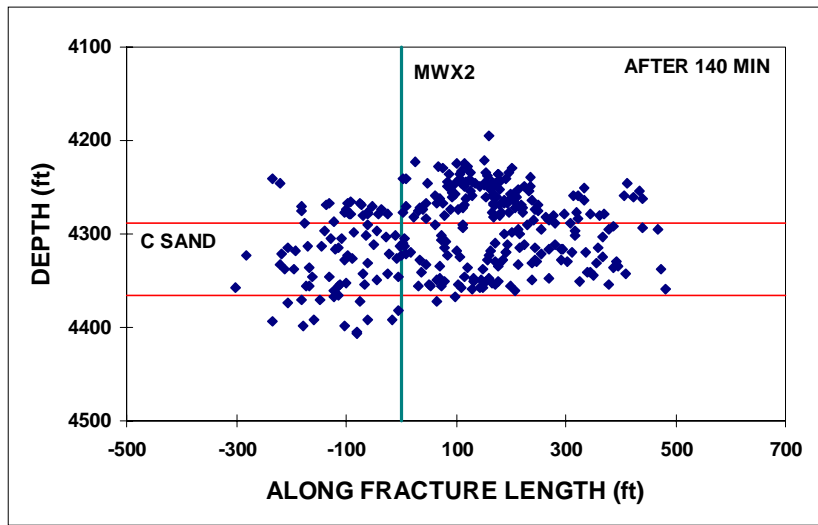


Figure 53. Side view of injection 4C microseisms recorded after 140 minutes of testing.

The microseisms recorded up to shut in are shown in Figures 54 and 55. Almost all of the activity is on the east wing, which shows a progressive lateral extension. At this time the east wing length is at least 600 ft. The fracture has also achieved its final height profile at this time.

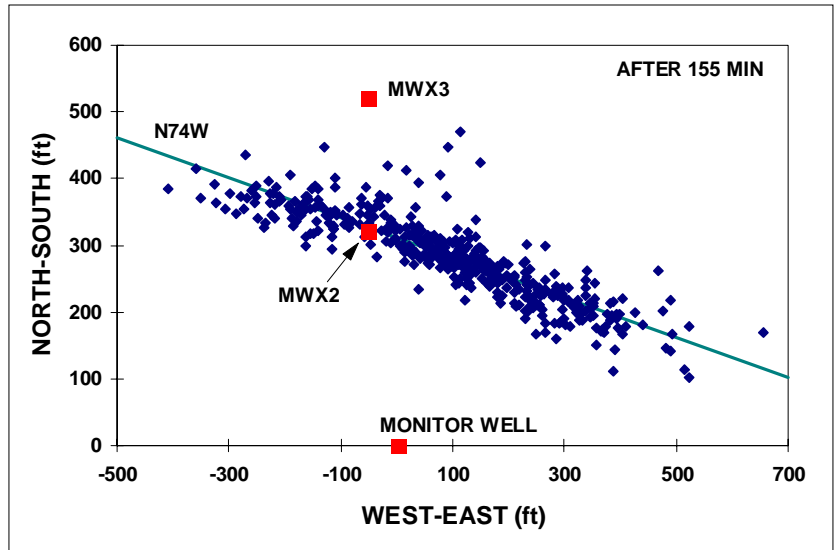


Figure 54. Plan view of injection 4C microseisms recorded after 155 minutes of testing.

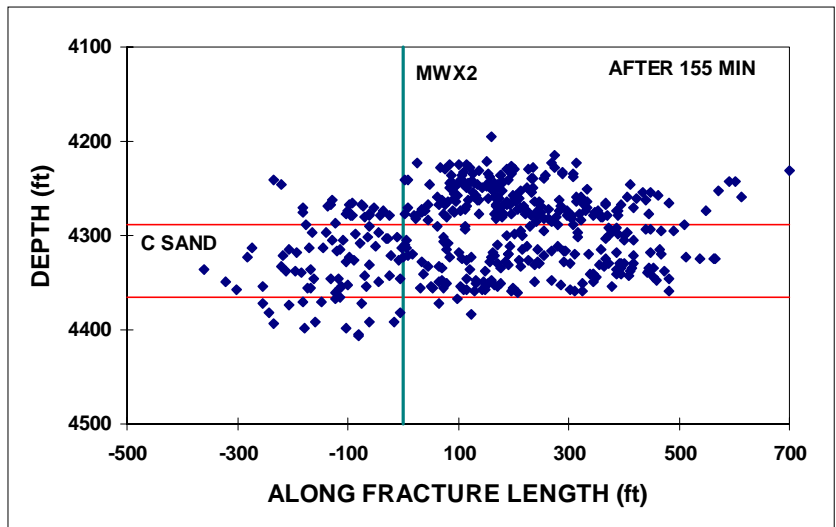


Figure 55. Side view of injection 4C microseisms recorded after 155 minutes of testing.

Injection 4C was a very complex fracture with several asymmetries in growth. The microseismic results may change slightly, as none of these data had a final quality control check at the time of this report. Some of the outliers may move or disappear if a reason for error are found. Details of the intersection, pressure drops, and other important details of this test will be finalized in 1997.

8.3.8 Injection 5C and 6C

Injections 5C and 6C were conducted on December 17 and 19, respectively. Injection 5C was a repeat treatment well test, but this time with the receiver string below the perforated interval in order to minimize vibrations to the receivers. Approximately 650 bbl of crosslinked gel was injected at 30 bpm while monitoring from both the treatment well and the monitor well. These results were not analyzed during 1996 and will be completed in 1997.

Injection 6C was an industrial size treatment, consisting of 1750 bbl of crosslinked gel and 250,000 lb of sand pumped at 30 bpm. Microseisms were detected from the monitor well array and from a limited array in the wireline well (MWX-3). Although it was originally planned to have a full 5-level array in MWX-3, the extreme cold temperatures during this test period caused considerable communications problems and only one or two levels actually provided any information during the test. These data will also be analyzed in 1997.

9.0 MICROSEISMIC PROCESSING

In order for microseismic diagnostics to become a usable field service, it will be necessary to develop automatic processing algorithms to map event locations on a real-time or near-real-time basis. The primary code for automatic processing of the microseismic data is SMART5. During 1995, SMART5 was built so that it would accurately detect p-wave arrivals. While 5-level p-wave data are sufficient to accurately locate microseisms in homogeneous formations, it was found that layering causes enough errors that s-wave data are also required for accurate locations. The methodology for implementing s-wave analysis in SMART5 was begun in 1996.

9.1 Additions to SMART5

Initial analysis of the typical microseisms detected at M-Site have provided information to develop a methodology for s-wave detection. All of the s waves detected have either

- greater amplitude than the surrounding codas of other waves,
- lower frequency than the p wave and its coda, or
- near-90° shift in particle-motion phase.

These differences are being implemented in an s-wave detection scheme where each feature is weighed and provides a vote on s-wave arrival. At least two confident votes are required to declare an s wave. Actual completion of the s-wave implementation will take place in 1997.

9.2 Adaptation of Vidale-Nelson algorithm

The Vidale-Nelson algorithm has been chosen as the analysis code for microseismic locations in complex velocity-structure environments. This code was described in detail in the previous annual report. During 1996, however, the porting of this code to the PC environment began and attempts were made to simplify the execution of the code by developing a simple front end for the five separate codes that make up this algorithm. The porting was completed in 1996 and an initial version of the front end has also been developed.

10.0 OTHER DIAGNOSTIC TASKS

10.1 Re-Design of 5-Level Circuitry

One of the major tasks undertaken in 1996 was a re-design of much of the circuitry in the 5-level system. This re-design was brought about by the poor performance of the 5-level system during the B sandstone experiments at M-Site. Boards from several receivers were sent to Sandia by Bolt for inspection. It was found that the high temperature printed circuits had been poorly soldered and many of the connections were marginal and subject to disconnect during any mechanical vibration. Sandia then developed a redesign of the A/D, signal processing, and motor control boards using low-temperature solder and components. The switch to low-temperature was a decision made based upon the inability of untrained workers to perform adequate high-temperature soldering. Any field or shop replacement of components would have likely been difficult as long as high temperature solder was used. Furthermore, it was expected that 90% of all fracture treatments could be accommodated with low-temperature solder and components.

All three printed-circuit boards were redesigned and populated with the same or equivalent components as the previous design, but a number of modifications were also made to the boards to improve performance and reliability. These boards were completed in April of 1996 and sent to Bolt for installation in the receivers.

A check of the receivers' performance was made in a test conducted at Texaco's Humble test facility, where downhole and surface airgun shots were detected at depths of 2000 ft and distances of 800 ft. Performance of the receivers was excellent, but some problems were still noted with communications between the receivers and the DAS-1 controlling the system. Nevertheless, the tool string was judged to be in excellent condition for microseismic testing.

10.2 UPRC Carthage Test

Sandia has been participating in the UPRC Carthage Test in the Cotton Valley sandstones. This is a complicated diagnostic test using two monitor wells, both with cemented tri-axial geophone arrays. Assistance is being provided in experiment design and analysis.

11.0 REFERENCES

1. Warpinski, N.R., Teufel, L.W., Lorenz, J.C. and Holcomb, D.J., "Core Based Stress Measurements: A Guide to Their Application," GRI-93/0270, June 1993.
2. Hill, R.E, Peterson, R.E., Warpinski, N.R., Lorenz, J. and Teufel, L.W., "Techniques for Determining Subsurface Stress Direction and Assessing Hydraulic Fracture Azimuth," GRI-93/0429, November 1993.
3. Warpinski, Z.A. Moschovidis, C.D. Parker and I.S. Abou-Sayed, "Comparison Study of Hydraulic Fracturing Models: Test Case - GRI Staged Field Experiment No. 3," SPE Production and Facilities, Vol. 9 pp.7-12, February 1994.
4. Warpinski, N.R., Abou-Sayed, I.S., Moschovidis, Z. and Parker, C., "Hydraulic Fracture Model Comparison Study: Complete Results," GRI-93/0109, Gas Research Institute Report, February 1993.
5. Warpinski, N.R., "Interpretation of Hydraulic Fracture Mapping Experiments," SPE 27985, Proceedings, Tulsa Centennial Petroleum Engineering Symposium, Tulsa, OK, pp. 291-300, August 1994.
6. Lorenz, J.C. and Laubach, S.E., "Description and Interpretation of Natural Fracture Patterns in Sandstones of the Frontier Formation along the Hogsback, Southwestern Wyoming," GRI-94/0020, January 1994.
7. Lorenz, J.C., Arguello, J.G., Stone, C.M., Harstad, H., Tuefel, L.W., and Brown, S.R., "Predictions of Fracture and Stress Orientations: Subsurface Frontier Formation, Green River Basin," GRI-95/0151, April 1995.
8. Biffle, J.H., "JAC3D - A Three Dimensional Finite Element Computer Program for the Nonlinear Quasi-Static Response of Solids with the Conjugate Gradient Method," SAND87-1305, Sandia National Laboratories, Albuquerque, NM, 1987, Reprint 1995.
9. Warpinski, N.R., Engler, B.P., Young, C.J., Peterson, R.E., Branagan, P.T. and Fix, J.E., "Microseismic Mapping of Hydraulic Fractures Using Multi-Level Wireline Receives," SPE 30507, Proceedings, SPE Annual Technical Conference, Dallas, TX, October 22-25, 1995.
10. Peterson, R.E., Warpinski, N.R., Wright, T.B., Branagan, P.T. and Fix, J.E., "Results of M-Site Experimentation in the A-Sand Interval: Fracture Diagnostics, Fracture Modeling and Crosswell Tomography," GRI-95/0046, February 1995.
11. Branagan, P.T., Peterson, R., Warpinski, N.R. and Wright, T.B., "The Characterization of Remotely Intersected Set of Hydraulic Fractures: Results of Intersection Well No. 1: GRI/DOE Multi-Site Project," SPE 36452, SPE Annual Tech. Conf. & Exhibition, Denver, CO, Oct. 6-9, 1996.
12. Branagan, P.T., Warpinski, N.R., Engler, B.P., Wilmer, R., "Measuring the Hydraulic Fracture-Induced Deformation of Reservoir and Adjacent Rocks Employing a Deeply Buried Incliner Array: GRI/DOE Multi-Site Project," SPE 36451, SPE Annual Tech. Conf. & Exhibition, Denver, CO, Oct. 6-9, 1996.
13. Peterson, R.E., Wolhart, S.L., Frohne, K.-H., Warpinski, N.R., Branagan, P.T. and Wright, T.B., "Fracture Diagnostics Research at the GRI/DOE Multi-Site Project: Overview of the Concept and Results," SPE 36449, proceedings, 1996 SPE Annual Tech. Conf. and Exhibition, Denver, CO, October 6-9, 1996.
14. Warpinski, N.R., Wright, T.B., Uhl, J.E., Engler, B.P., Drozda, P.M. and Peterson, R.E., "Microseismic Monitoring of the B-Sand Hydraulic Fracture Experiment at the DOE/GRI Multi-Site Project," SPE 36450, proceedings, 1996 SPE Annual Tech. Conf. and Exhibition, Denver, CO, October 6-9, 1996.

12.0 MAJOR ACHIEVEMENTS

Major achievements include:

Completion of all M-Site B sandstone microseismic analyses and the preparation or participation in four SPE papers describing the results of the experiments.

Finite element analyses of the inclinometer results from the M-Site B sandstone experiments. Results from these analyses show that the B sandstone microseismic data are accurate representations of the fracture height, thus validating this aspect of the technology. Furthermore, the finite element analyses showed that modulus variations have a significant effect on the inclinations and the failure of the analytic models to accurately match the data is due to the layering.

The first of several technology-transfer seminars on M-Site B sandstone results.

A complete re-design and fabrication of A/D, signal-processing, and motor-control circuit boards for the 5-level receiver system. This reconstruction of the receiver boards solved problems with shoddy workmanship on the high temperature soldering of the previous set of boards. Acceptability of the new boards and the re-worked system were tested at Texaco's Humble facility.

Planning and execution of six M-Site C sandstone experiments using microseismic, inclinometer, and intersection-well diagnostics to monitor fracture growth and behavior.

Complete analysis of the 1C, 2C and 3C microseismic results from both the monitor well and the 5-level well. Results show that the microseismic length agrees with the time a pressure increase was observed in the intersection well, thus validating the microseismic length. The results also show that the 5-level receiver data agree favorably with the monitor well data.

The porting of the Vidale-Nelson algorithm to the personal computer environment for on-site application. This code calculates accurate microseism locations in layered environments where velocity structure is significant.

13.0 MAJOR PROBLEMS

The major problem during 1996 was the necessity to re-fabricate the receiver circuit boards. However, this task was successfully completed and the receiver string was available by June 1996.

A secondary problem dealt with funding of the M-Site C sandstone experiments, causing delays in the experiments. A decision by the site operator to not make the site available for testing in 1997 forced a rapid completion of the testing.

14.0 CONCLUSIONS

The M-Site B sandstone experiments , which were documented in four SPE papers, showed that microseismic analyses provide accurate information on fracture height and fracture azimuth. Both of these geometric parameters were validated using other independent techniques. Fracture height was validated with downhole inclinometers, which measure the deformation of the rock mass in response to the fracture (the mechanical response). Fracture azimuth was verified by intersecting the fracture with a deviated well. B sandstone experiments again showed a pattern of rapid lateral growth and well contained fracturing until net pressures became large enough to support height growth.

Results from finite-element analyses of the M-Site B-sandstone have been important for understanding the inclinometer responses. These finite element analyses showed that modulus variations have a significant effect on the inclinations and the failure of the analytic models to accurately match the data is due to the layering.

Re-design and fabrication of A/D, signal-processing, and motor-control circuit boards for the 5-level receiver system were completed in 1996. Acceptability of the new boards and the re-worked system were successfully tested at Texaco's Humble facility.

Six M-Site C sandstone experiments were successfully completed in 1996. These experiments used microseismic, inclinometer, and intersection-well diagnostics to monitor fracture growth and behavior. Analysis of the 1C, 2C and 3C microseismic results from both the monitor well and the 5-level well were completed in 1996, and initial analysis of the 4C experiment was also performed. Results show that the microseismic length agrees with the time a pressure increase was observed in the intersection well, thus validating the microseismic length. The results also show that the 5-level receiver data agree favorably with the monitor well data. Rapid lateral growth in the sandstone was again observed, but primarily during the injection of low viscosity fluid.

15.0 OBJECTIVES AND WORK PLANNED FOR NEXT YEAR

Completion of all C sandstone analyses and preparation of reports and SPE papers documenting these results will be a major task for 1997.

1997 will be the year when joint industry-GRI tests of the microseismic diagnostic technology begins. Industry partners will be sought out and joint tests conducted using the 5-level string. Analysis of these tests will be performed primarily by the SMART5 code (real-time) and the Vidale-Nelson algorithm (post-processing).

Techniques for automatically detecting the s-wave arrival will be fully implemented in 1997 and incorporated into SMART5.

The 5-level system, which is a highly complex receiver string, will continue to be supported. One of the major needs is an on-site diagnostic system for assessing problems that develop. Currently, there is no diagnostic system which allows for any estimation of technical problems. Sandia will begin to develop several levels of diagnostic support for this system.

Sandia will continue to support and advocate the use of downhole tiltmeters for various hydraulic-fracturing operations. If it fits into any of the joint industry-GRI tests, an attempt will be made to run a single, wireline-run, downhole tiltmeter in one of the tests.